Journal Pre-proof

Seismic risk assessment of an existing oil refinery subjected to earthquake swarms

Armin Majidian , Luigi Di-Sarno

PII: S0951-8320(25)00682-9
DOI: https://doi.org/10.1016/j.ress.2025.111482
Reference: RESS 111482

To appear in: *Reliability Engineering and System Safety*

Received date: 19 March 2024
Revised date: 17 July 2025
Accepted date: 19 July 2025

Please cite this article as: Armin Majidian , Luigi Di-Sarno , Seismic risk assessment of an existing oil refinery subjected to earthquake swarms, *Reliability Engineering and System Safety* (2025), doi: https://doi.org/10.1016/j.ress.2025.111482

Highlights

- Components showing aging effects are most vulnerable to failure during the initial stages of damage under earthquake swarms.
- Structural components are more susceptible to severe damage compared to non-structural counterparts
- Corrosion impacts on severe damage levels are significant, regardless of whether they occur during the mainshock or aftershocks.
- Lack of maintenance planning coupled with the effect of aftershocks can slightly increase the life cycle costs of the structure.
- The combined impact of corrosion and aftershocks can halve the resilience of the structure, compromising its structural integrity.

.

Seismic risk assessment of an existing oil refinery subjected to earthquake swarms

Armin Majidian[a,*] and Luigi Di-Sarno[a]
[a] *Department of Civil and Environmental Engineering, University of Liverpool, United Kingdom;*

Abstract

Steel oil refineries are subject to ageing due to corrosive chemicals and harsh atmospheric conditions, leading to the degradation of their structural integrity. This deterioration affects the resilience of process units against seismic events, particularly during strong aftershocks. Leaks in pipelines or damage to tanks containing hazardous materials pose health risks and can necessitate shutdowns for essential repairs. Hence, maintaining the integrity and safety of both structural and non-structural components and adopting a proper maintenance plan is essential. This paper investigates the performance of a petrochemical unit in a seismic area, estimating damage risks from earthquake swarms considering soil-structure interactions and damage accumulation. Fragility curves, based on defined damage states, were developed to create a customized risk assessment model for oil refineries. A life cycle cost analysis was also conducted, considering an effective corrosion maintenance plan over the lifetime of the structure. The results showed that inadequate maintenance and aftershocks, increase life cycle costs by 2% for uncorroded structures and 4% for corroded structures due to aftershocks. The combined effects of aging and aftershocks significantly increase annual failure rate and reduce structural resilience. Corroded structures under sequence motions face the highest failure risk, with a 1,000-year return period at low damage level. Aftershocks further decrease resilience by 2% and double the annual slight damage rate under sequence motions. The results also reveal that structural components are more prone to damage than non-structural ones. The proposed framework systematically evaluates seismic risk and resilience in refinery units under harsh atmospheric conditions.

Keywords: Natech, Probabilistic risk assessment; Refinery unit; Corrosion; Seismic sequence; Seismic resilience

1. Introduction

1.1. Background

Consolidated research outcomes have indicated that major accidents in industrial plants can result in significant damage to equipment and endanger the health of workers [1] .This is due to the presence of toxic and often flammable materials, which jeopardize the overall safety of oil refineries. A recent study revealed that 28% of major industrial accidents are related to process plants, leading to human injuries, environmental damage (e.g. soil contamination, water and air pollution), equipment loss (e.g. process equipment, storage tanks), and financial loss [2]. Approximately 15.5% of such accidents occurred due to earthquake motions according to Natural hazard-triggered technological accidents (Natech) database [3]. In the last two decades, the petrochemical and oil refineries recorded the highest number of accidents,

[*] Corresponding author.
E-mail: a.majidian@liverpool.ac.uk (A. Majidian)

highlighting the importance of studying and assessing the performance of these industrial sectors to prevent potential damage and significant losses in future [4].

Previous industrial incidents have shown that Na-tech events caused by geophysical disasters have the highest likelihood of causing damage to human and assets. [5]. Strong ground motions as one of the most destructive agrophysical events can endanger the safety of structures and undermine health of people by causing widespread damage to both structural and non-structural components. The statistical data indicate that total repair cost of earthquake damage from 2,000 is around $400 billion with approximately 530,000 deaths and 1,500,000 injuries [6]. The damage can be more destructive in industrial process units. Many earthquake reconnaissance surveys have assessed the damage and loss of industrial facilities after major strong motions [7–9]. For example, in 2011 Tōhoku earthquake with magnitude M_w=9, an oil refinery with several storage tanks was damaged. This led to failure of diagonal braces supporting the tank legs, resulting in the collapse of the tanks during subsequent aftershock with a magnitude of 7.9. The leakage from the pipes containing the flammable liquid resulted in several explosions [4,7]. Hence, assessing the seismic performance of existing petrochemical and refinery plants in high-seismicity areas for implementation of effective protection techniques and provide appropriate cost-effective maintenance plan is crucial.

Petrochemical plants transfer and store chemical liquids and gases under high-pressure and temperature conditions, making structures vulnerable to corrosion attacks. The estimated annual cost of corrosion in U.S. industrial plants in 2013 was around $137.9 billion with 12.8% of this total ($17.6 billion) was for production and manufacturing industries. Petroleum refinery units accounted for 21% of this value ($3.7 billion) [10]. Without adequate protection techniques and a regular maintenance plan, petroleum refineries can experience different types of corrosion, depending on the materials used and the environmental conditions. [11]. Different methods can be employed to decrease the corrosion rate in petroleum refinery assets, e.g. utilizing coatings and employing inhibitors. The choice depends on corrosivity of raw materials, temperature, pressure and chemical processes conducted within the unit [12]. In hydrotreating units which are responsible for removing the sulphur or nitrogen from raw materials, the presence of corrosive contaminants, such as hydrogen sulphide (H_2S), can increase significantly corrosion rate. In some cases, this can result in the formation of acid salts, leading to corrosion within the refinery unit. Corrosion can decrease the strength capacity of the corroded elements resulting to decreasing the global capacity of the entire plant. Investigating the vulnerability of aged refinery units is important to mitigate the probability of damage.

Numerous studies have focused on the seismic evaluation of refineries under seismic loads [13–21]. For example, a recent study investigated the seismic vulnerability of two unanchored cylindrical steel liquid storage tanks [15]. The study considered hydrostatic pressure and sloshing effects of the liquid on the wall shell and investigated the seismic response of the tanks using three-dimensional finite elements, with a particular focus on the effect of uplift. In another recent study, fragility assessment of a pipe-rack system, considering soil-structure properties was investigated. The study revealed that soil deformability plays a crucial role in the fragility assessment, influencing the seismic integrity of the pipe-rack system [19]. The seismic behaviour of cylindrical pressure vessels was studied using three-dimensional finite element methods, considering sloshing effect [14]. The results indicate that additional safety measures are required in seismic design of pressurized vessels. A recent study introduced a comprehensive virtual refinery testbed for system-level seismic risk assessment, offering detailed asset-level modelling and a homogenization framework to translate individual asset damage into global operational disruption and hence supporting resilience-focused evaluations [22]. In another numerical investigation, researchers studied the effect of aftershock motions on risk assessment of an existing petrochemical plant with aging effect [23]. It was shown that corrosion affect more significantly the risk of damage and loss compared to aftershocks, and impact of aftershocks is heightened in corroded structures. Seismic performance of industrial moment-resisting frames with process secondary components through full-scale shaking table tests was recently studied [21]. The results highlight the dynamic interaction between primary and secondary structures and the need for localized retrofitting to mitigate damage in industrial facilities.

Seismic risk is a well-established concept in earthquake engineering used to evaluate the risks associated with earthquakes. A widely adopted approach for seismic risk assessment is outlined in the Pacific Earthquake Engineering Research (PEER) Centre Seismic Risk Assessment Framework, which includes hazard characterization, structural response analysis, damage and loss estimation, and decision-making process [24]. Traditional seismic risk assessment primarily focuses on assessing the immediate impact of an earthquake. However, this approach often does consider the long-term effects such as recovery process after earthquake or its ability to adapt to future sequential earthquakes. Seismic damage to large-scale infrastructure (e.g. chemical plants) can lead to not only substantial direct economic losses (e.g. repair costs) but also prolonged indirect losses. The losses arise from factors such as reduced functionality due to successive hazards, aging effects, and the interdependencies within distributed infrastructure systems [25,26].

To address these limitations, seismic resilience assessment has emerged as an extension of seismic risk assessment, placing greater emphasis on evaluating the time-dependent functionality trajectories making it a crucial tool for assessing and optimizing long-term mitigation and restoration strategies in industrial plants [27–30]. By incorporating resilience-based metrics, provides a more comprehensive understanding of how the entire process plant can recover and adapt over an extended planning horizon, ultimately improving disaster preparedness and risk management in process plants.

1.2. Research workflow and objectives

The present study employs probabilistic seismic risk assessment to estimate the damage, loss and the resilience of a typical aged petroleum unit subjected to earthquake motions. A series of comparative analyses were conducted to evaluate the long-term impact of aging and aftershocks on seismic vulnerability and performance. Finite element methods (FEMs) are utilized to numerically model the case study structure, subjecting it to natural earthquake through response-history analyses. The sections provided hereafter start with a brief overview of corrosion mechanism and available corrosion time-dependant models in the literature. This is followed by the summary of methodology used in conducting seismic risk assessment, damage and loss analysis, and resilience evaluation. The research roadmap is illustrated in Fig. 1, which highlights the fundamental steps that contribute to robust and efficient decision-making process.

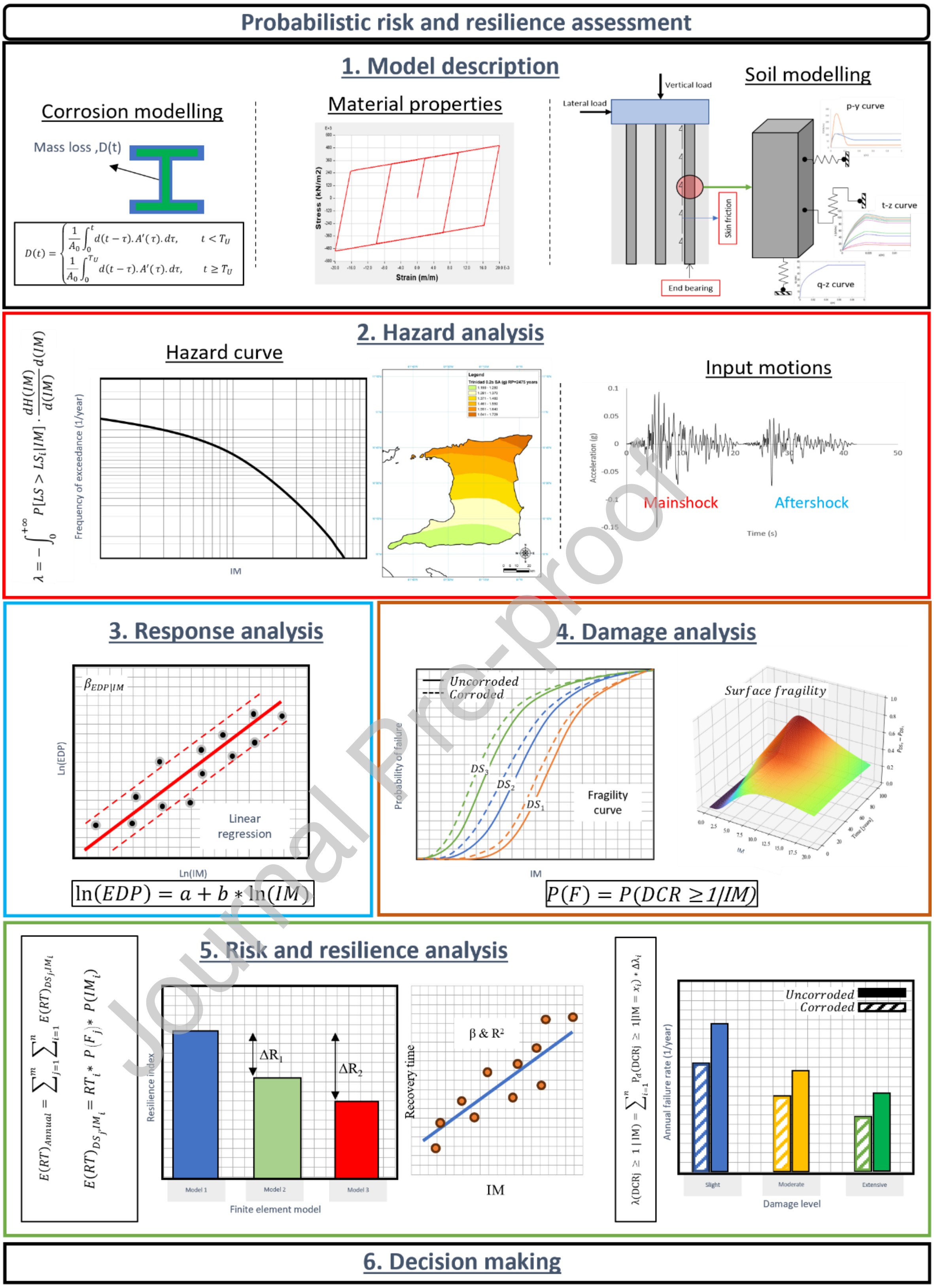

Fig. 1 . Research roadmap

The outcomes of the framework in Fig. 1 provide valuable insights for researchers, insurance companies, and industry stakeholders, enabling more effective structural monitoring over the lifetime of the facility through probabilistic risk and resilience assessment. By incorporating relevant uncertainties, accounting for ground motion variability and uncertainty in limit state thresholds affecting demand and capacity assessments, this approach enhances the reliability and safety of complex petrochemical systems, supporting more informed maintenance strategies and emergency response planning. The results contribute to improved resilience, extended service life, and enhanced risk mitigation during seismic events. This study focuses on system-level performance metrics and does not explicitly model physical consequences.

2. Corrosion in oil refineries

Corrosion, leading to equipment integrity loss through general or localized thinning of steel shells, can result in leaks or ruptures. Internal process conditions like high temperatures or aggressive substances, coupled with other factors such as humidity or proximity to saline environments, can increase the severity of corrosion [31]. Petrochemical units transmit the crude oil to refined oil for various fuel types. Such process exposes industrial equipment and supporting structures to aggressive condition, leading to corrosion [11].

Crude oil is stored in storage tanks before being transferred to process units, and corrosion in tanks can derive from factors like water accumulation or damage of the outer protection layer. Presence of salts can increase the risk of pitting corrosion caused in industrial plants. Desalting units aim to remove inorganic salts (e.g. H_2S, Na_2S) from the material. Distillation columns separate refined materials from raw materials based on different boiling points. Hydrotreating units are critical sections of refinery, responsible for removing sulphur and nitrogen compounds from petroleum materials to ensure that they meet the environmental standard levels. In reactors, dissolved acid gases like H_2S are removed, entering liquid/gas separators where sulphur gas can create acid salts, causing uniform corrosion in carbon steel [32]. The corrosion rate in a refining unit is significantly influenced by relative humidity (RH), measured at around 1.35 millimetres per year at 80% RH for carbon steel in a temperature of 50 degrees Celsius [21].

Refineries can experience a variety of failure modes across critical components during earthquake. Pipes encompass issues with the rigidity of support-to-pipe connections, the vulnerability of fractured fittings at T-joints due to equipment movements and pipe vibrations. The failure of a vessel in a refinery unit which can lead to pipes failure. Supporting structures can experience damage, such as failures in structures supporting pipes, anchorage, and collapses of rack supports [33]. These failure modes underscore the necessity for robust safety measures to protect refinery operations.

2.1. Corrosion models

The extent of corrosion damage is greatly affected by the environmental conditions where structures are originally constructed [34]. Various factors including rainfall patterns, relative humidity, temperature, the presence of pollutants like SO_2, airborne salinity (chloride ions), pH levels in seawater, and wind speed can significantly affect the determination of corrosion rate during the service life of the structure [35–37]. Especially when climate change data (such as temperature variation, humidity, pollutants, etc.) for a specific location is available, it facilitates estimating the long-term impact on corrosion rate, although this can be challenging in some cases. Rural regions, characterized by minimal aggressive contaminants, experience the minimum corrosion rate. In contrast, urban areas and coastal regions with moderate salinity levels are considered to have a moderate corrosivity. Inshore industrial facilities with medium and high level of salinity can be represented as high corrosivity classes. Structures located in marine and offshore environments face the most extreme conditions, characterized by the highest concentrations of contamination ions and acids, leading to the greatest rate of corrosion. International Organization for Standardization (ISO), assigns specific class for each corrosivity level, ranging from C1, indicating the least corrosive environment, to CX, related to the most corrosive environmental condition [34].

Corrosion appears in various types and forms [38–40]. Corrosion can occur either locally or uniformly across the entire metal surface. In atmospheric conditions, corrosion starts with localized form like pitting and without proper maintenance plan (e.g. repainting), and as a rust layer forms, the corrosion progresses to uniform thickness loss over long time. In other words, the decrease in the mass of steel components can be approximated as a uniform reduction in cross-sectional thickness. This reduction in thickness, can be quantified using time-dependent model as illustrated in (1). This model has been developed for different corrosivity classes based on empirical data gathered from various environmental conditions [41–44].

$$D(t) = D_0 t^n \tag{1}$$

where D_0 represents the average corrosion rate expressed in units of millimetres or micrometres per year, while n is the coefficient associated with the long-term impact factors and *D(t)* is the corrosion thickness loss after t years.

Numerous studies have integrated a variety of environmental factors to estimating the average corrosion rate [34,44]. For example, ISO 9223 model considers factors such as time of wetness, relative humidity, temperature, pollution, and air salinity. It also considers the interaction between these factors to provide an average value for corrosion rate. However, climate changes could alter in the future the environmental condition, potentially causing the actual corrosion rates to deviate from current average estimates. This highlights the significance of considering climate change factors in estimating corrosion rates over the lifetime of a structure which can greatly aid in decision-making and improve maintenance planning strategies [45]. Recently, several studies have utilized machine learning methods to develop models for the time-dependent corrosion rates of carbon steel [46,47]. The models can predict corrosion rates under various climate change conditions, thereby decreasing the reliance on extensive experimental procedures. These approaches can significantly contribute to more efficient and cost-effective corrosion management in industrial units.

Recently, a study has combined the deterioration rate of coating layer and metal corrosion rate to present a more comprehensive and realistic model [48]. In this study, the effect of localized corrosion was considered following the first damage (first scratch) to the coating layer, prior to the complete removal of the entire coating from the steel surface. Eq. (2) illustrates the time-dependent mathematical model and Fig. 2. Corrosion loss mechanism represents the mechanism of corrosion attack considering degradation of the coating layer.

$$D(t) = \begin{cases} \dfrac{1}{A_0}\displaystyle\int_0^t d(t-\tau).A'(\tau).d\tau, & t < T_U \\ \dfrac{1}{A_0}\displaystyle\int_0^{T_U} d(t-\tau).A'(\tau).d\tau, & t \geq T_U \end{cases} \tag{2}$$

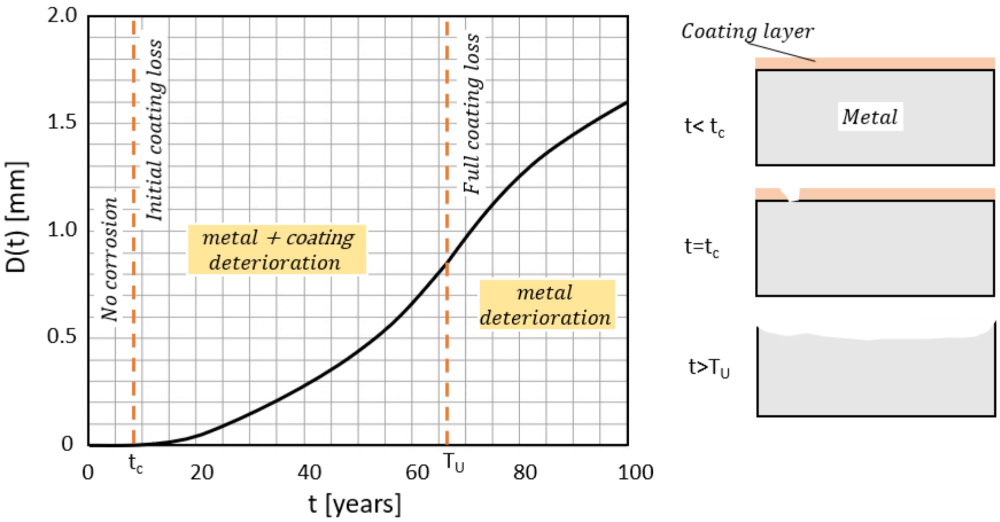

Fig. 2. Corrosion loss mechanism

where A_0 is the initial protective area and $A'(\tau)$ represents the rate of protection area loss over time τ. T_U indicates the life of the coating layer (complete degradation) which can be computed as 1.38*T_{50}, where T_{50} is the time required for half of the coating area to deteriorate [49]. The value of T_{50} varies, depending on the specific coating systems in use. t_c represents the duration which the element remains fully protected from corrosion, where $D(t)$=0.

The implementation of a comprehensive maintenance plan throughout the service life of the structure can enhance its overall integrity and safety. A study suggested a management strategy customized for each specific protective layer type [50]. This plan outlines maintenance activities over the lifetime of the structure, classified into three distinct phases: touching up layers, repainting damaged sections, and eventually repainting all elements.

Corrosion incidents within refinery units stand out as paramount concerns in both design and the formulation of consistent maintenance strategies. While numerous studies have focused on the impacts of corrosion alone, only a limited number have concurrently addressed the combined effects of corrosion and seismic activities on structural integrity [51,52]. With appropriate design, refinery equipment and primary structures are intended to either remain undamaged or sustain only slight damage, ensuring the safety of refinery workers. Nonetheless, corrosion can elevate the risk profile by altering the capacity of the system. Consequently, in the event of an earthquake followed by strong aftershocks, the structural and non-structural elements may become increasingly susceptible to the seismic sequence, particularly if they have already been compromised by corrosion.

3. Methodology

To assess the risk during earthquakes, structural responses should be analysed at various intensity measures and the probability of damage at specific performance levels, such as life safety or collapse prevention, should be determined. A common method for identifying the responses is regression analysis, which is also referred to as Cloud analysis, assuming that the seismic response follows linear logarithmic distribution [53]. The equation derived from this analysis is represented as Eq. (3)&(4):

$$ln\,(EDP_M) = lna + b * ln(IM) \quad (3)$$

$$\beta = \sqrt{\sum_{i=1}^{N} \frac{(ln(EDP_i) - ln(EDP_M))^2}{N-2}} \quad (4)$$

where a and b are the coefficients for the regression line, while EDP_M indicate the median value of the Engineering Demand Parameter (EDP) that represents the structural response to seismic motions. IM stands for Intensity Measure, reflecting the severity of earthquake and β denotes the standard deviation in lognormal data. N denotes the number of ground motion records evaluated in the analysis. Examples of EDPs include the Maximum Inter-story Drift Ratio (MIDR), maximum joint rotation (θ_{max}), Maximum floor acceleration (Acc_{max}), and Maximum Hysteresis Energy dissipated during earthquake. Spectral Acceleration at the first mode ($Sa(T_1)$), Peak Ground Acceleration (PGA), and Arias Intensity (AI) are the examples of intensity measure which commonly use in structural analysis.

Probability of a structure reaching a certain level of damage, referred to as the fragility function, is typically represented by the lognormal cumulative distribution function (CDF) of the cloud data, as shown in Eq. (5):

$$P(F_j) = P(DCR_j \geq 1 \mid IM) = \Phi\left(\frac{ln(EDP)}{\beta_j}\right) \quad (5)$$

where $P(F_j)$ represents the probability of a structure experiencing failure or reaching a specific damage state j. The parameter DCR stands for the Demand (response) to Capacity Ratio associated with each damage state. The function $\Phi(.)$ denotes the standard normal distribution.

Considering the effects of aftershocks, Eq. (5) should be modified to account for both mainshock and aftershock motions. This is achieved by evaluating the response conditioned on the intensity of mainshock motions (IM_{MS}) and the expected aftershock intensity (IM_{AF}), as detailed in Eq. (6). Accordingly, the structural response is adjusted, considering the algebraic relationship between the responses to mainshocks and aftershocks, as shown in Eq. (7).

$$P(DCRi \geq 1 \mid IM_{MS}) = \Phi\left(\frac{ln(EDP_{MSAF})}{\beta_i}\right) \quad (6)$$

$$EDP_{MSAF} = EDP_{MS} + EDP_{AF} \quad (7)$$

where EDP_{MSAF} indicates the estimated response of the structure when subjected to seismic sequence, and EDP_{AF} denotes the response of a structure, which has already been damaged by the mainshock, to sequence motions.

To evaluate the seismic risk of the structure at a particular damage state j, the risk metric known as annual failure rate (λ) can be determined. λ can be calculated by integrating the fragility function with the seismic hazard characteristics of the study location as stated in Eq. (8):

$$\lambda(F) = \sum_{i=1}^{n} P(DCRj \geq 1 | IM = x_i) * \Delta p(IM_i) \quad (8)$$

where $\Delta p(IM_i)$ represents incremental hazard rate associated with the intensity measure level x_i.

Identifying recovery time in seismic risk assessment is crucial specially in industrial units as it determines how quickly an infrastructure can return to normalcy after an earthquake. It helps in planning for post-disaster response and repair of critical infrastructure components. Seismic resilience is a measure of both ability of the system to withstand earthquake damage and its capacity to recover functionality over time. Enhancing resilience helps minimize the long-term social and economic impacts of seismic events, as it ensures a structure can recover functionality efficiently [54,55]. Calculating the expected annual recovery time ($E(RT)_{Annual}$), as indicated in the Eq. (9), involves estimating independent recovery times (RT) for various damage states (DS) and integrating these estimates with seismic risk assessments as outlined in Eq. (10). This integration combines the probabilities of encountering different seismic intensities ($P(IM_i)$) with the likelihood of surpassing specific damage thresholds ($P\left(F_j\right)$). The resilience index (R) can be calculated as the inverse of expected annual recovery time, accounting for both damage and its consequences. The comprehensive approach represents a structured method to quantify the total time required for a structure to recover from seismic events over a year, considering both the severity of potential damages and the frequency of seismic occurrences.

$$E(RT)_{Annual} = \sum_{j=1}^{m} \sum_{i=1}^{n} E(RT)_{DS_j, IM_i} \tag{9}$$

$$E(RT)_{DS_j, IM_i} = RT_i * P\left(F_j\right) * P(IM_i) \tag{10}$$

Estimating the costs throughout the service life of an asset is essential for informed decision-making. Life Cycle Costing (LCC), is defined as an analytical framework to measure the cumulative costs associated with a structure throughout its lifetime [56]. By employing LCC, engineers can refine design approaches to maximize cost-effectiveness, anticipate long-term maintenance plans, and balance initial budget with probable future expenses. This approach considers both the initial cost of construction and the maintenance costs during the life of the asset, as outlined in, as detailed in Eq. (11).

$$NPV = C_0 + \sum_{t=0}^{N} \frac{C_t}{(1+d)^t} \tag{11}$$

where *NPV* refers to the Net Present Value, representing the value of all future cash flows over the entire life of an asset. The variable C_t represents the costs incurred at year t, including maintenance, repair, or replacement costs. The discount rate, d, is utilized to adjust future costs to their present-day equivalent. This adjustment is executed by multiplying C_t with the appropriate reduction factor. The term C_0 represents the initial costs, such as design and construction costs, along with the costs associated with application of a protective coating layer on steel surfaces.

This methodology strengthens life extension strategies for petrochemical facilities in harsh atmospheric conditions, playing a crucial role in industrial safety and sustainability.

4. Asset at risk (case study)

In the present study, an irregular steel desulphurisation refinery unit located in a high-seismicity region of the Caribbean (coordinates: 10°18'54.9"N, 61°26'43.5"W) was assessed. This facility plays a crucial role in purifying diesel by removing sulphur, ensuring the final product meets acceptable sulphur content levels. As illustrated in Fig. 3-a, refinery unit comprises both horizontal and vertical vessels and steel pipes which are supported by a steel structure. The initial stage involves processing crude oil within the vessels for hydrotreating to remove the sulphur. Subsequently, the product is directed to reactor tanks for additional refining. The transportation of liquid between these components is facilitated through the steel pipes. Because of the presence of corrosive elements like hydrogen sulphide (H_2S) and other aggressive substances, along with the age of the unit, constructed fifteen years ago, structural integrity of the unit could be compromised over time due to aging effects such as corrosion.

The structure was constructed on clayey soil, as illustrated in Fig. 3-b, which exhibits three soil layers. The first layer, measured from the ground surface to approximately 4.8 meters below, is characterized by soft to medium-stiff silty clays, with a maximum shear velocity of around 207 m/s. The second layer, beneath the first layer with the width of 4.3 meters, comprises stiff to very stiff fissured silty soil with a maximum shear velocity of approximately 440 m/s. Below this layer, the soil consists of hard, silty clays, with a depth of 18.5 meters from the ground surface exhibiting a maximum shear velocity of around 530 m/s.

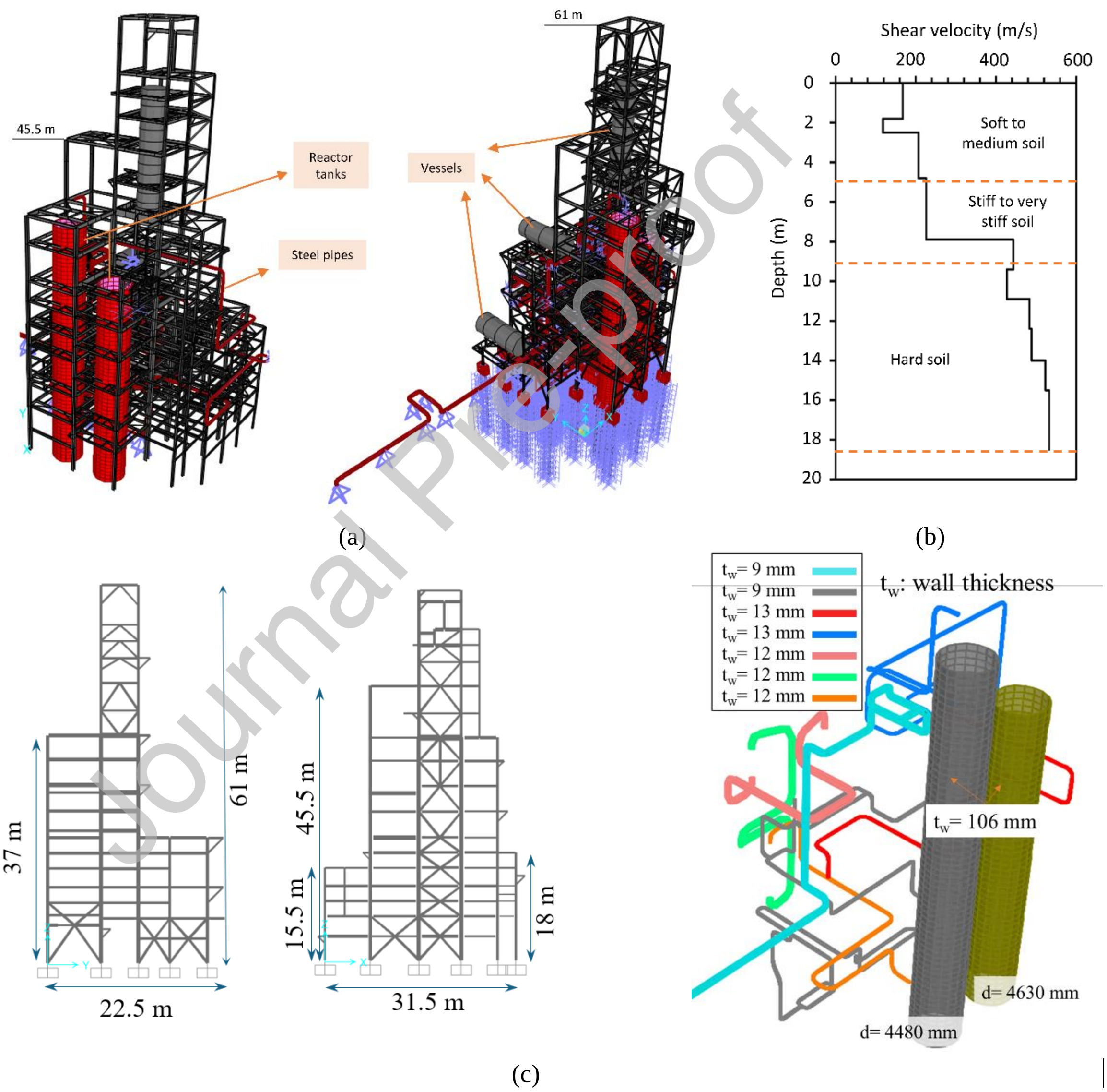

Fig. 3. (a) 3D finite element model of the asset, (b) soil profile, (c) model specifications.

The structural components (steel frame) were fabricated using ASTM A36/A36M steel grade [57], comprised ordinary moment frames (OMF) with some braces in Y direction and concentrated and chevron bracing system in X direction. Structural elements were designed with an expected yield capacity of 379 MPa and an ultimate yield capacity of 440 MPa with the modulus of elasticity of 203 GPa. The non-structural components (refinery process equipment), includes vessels, two reactor tanks, and transfer pipes run along the height of the building. Both steel tanks and vessels were constructed from the same material as the supporting steel frame. Two tanks, with 36 meters and 29 meters in height and each with a thickness of 106 millimetres, were supported by the steel frame. The seamless pipes with varying diameters, were made of ASTM A106 with expected yield capacity of 297 MPa and an ultimate capacity of 335 MPa. The diameter of the pipes varies, ranging from 200 millimetres to 600 millimetres.

(a)

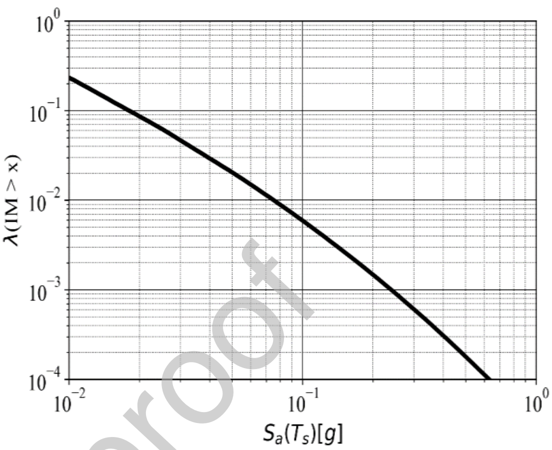

(b)

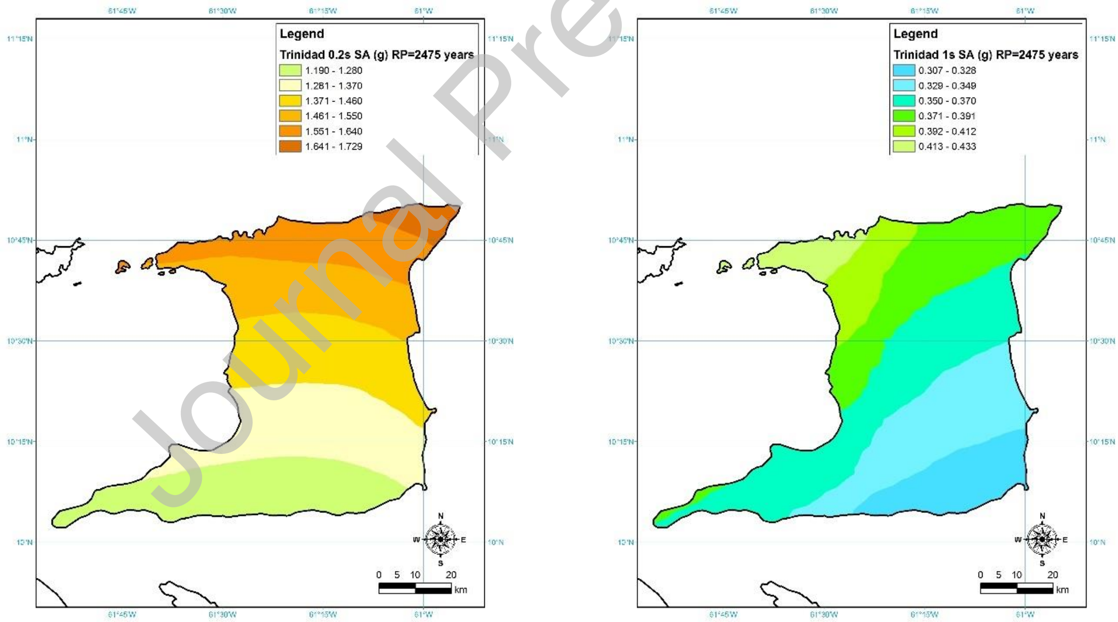

(c)

Fig. 4: (a) Active faults in the site of construction (South of Trinidad and Tobago); (b) seismic hazard curve and (c) seismic hazard maps of the study region.

The structure is located in a region with high seismic activity, including three faults in both near and far-field distances, as illustrated in Fig. 4-a&c. The short-period spectral acceleration (S_S) is measured at 1.37 seconds, and the long-period spectral acceleration (S_1), is recorded at 0.35 seconds [58]. Fig. 4-b shows the hazard characteristics of the case study location, illustrating the annual rate of occurrence for various earthquake intensity levels in the study region [59] . This curve was derived using probabilistic seismic hazard analysis (PSHA) [33].

The analysis of climate change and pollution rate changes for the case study location was conducted by studying the available statistical data over recent years [60]. The findings indicate that relative humidity level has remained relatively stable over the years, consistently averaging above 80%. This constant high humidity is a crucial factor in accelerating corrosion loss. In terms of air quality, pollutants such as SO_2, NO_2, and particulate matter (PM_{10} and $PM_{2.5}$) have been maintained at negligible concentrations, within the allowable limits. The annual concentration of CO_2 decreased since 2010. It is important to note that CO_2 in the presence of moisture can lead to acidic conditions that potentially increase the rate of corrosion. The data on temperature and annual rainfall indicate only minor changes over the years. Moreover, average wind speeds have varied slightly within this timeframe. Strong wind can accelerate the oxidation process, influence temperature fluctuations, and transport pollutants and particulate matter, all of which can impact the rate of corrosion. Fig. 5 provides a graphical representation of the variations in some of these parameters over time and real-time corrosivity level of the study region, which is classified as C5 level [61].

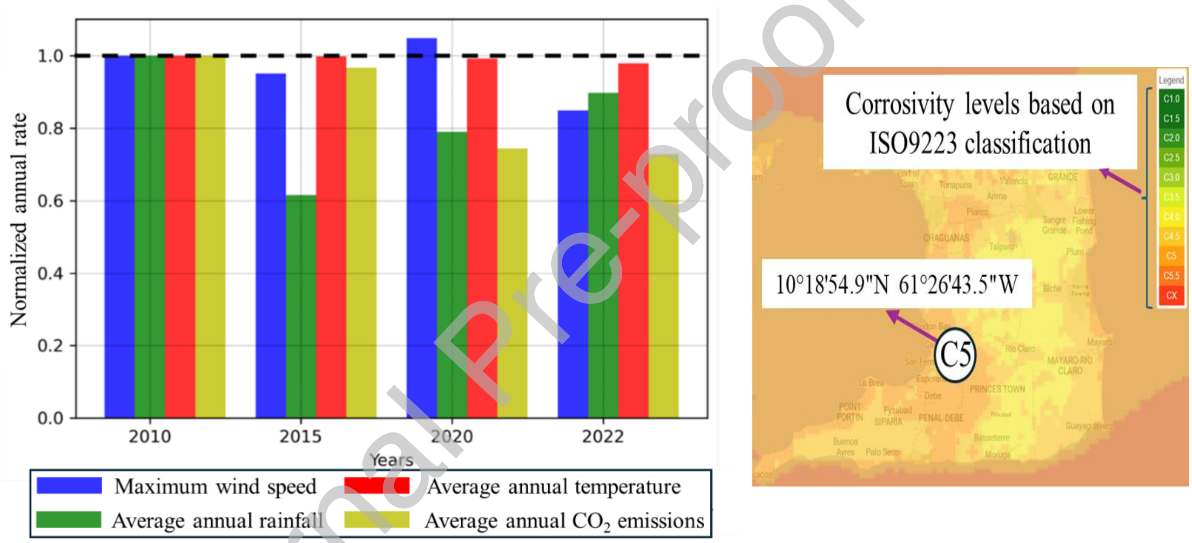

Fig. 5. (a) Normalized trends in climate change parameters over years. Each value is adjusted relative to its initial value for comparison and (b) corrosivity level of the study region

As illustrated in Fig. 5a, the effects of climate and air pollution trends have been relatively minor in recent years. While broader climate change impacts such as sea level rise and precipitation shifts are acknowledged in the literature [62], they are not directly incorporated into the numerical modelling in this study and are referenced solely for contextual background on long-term exposure conditions.

5. Numerical model

5.1. Finite element modelling

Finite element method (FEM) was employed to simulate the refinery unit using SAP2000 software [63]. Frame elements were defined with nonlinear hinges located at 5% and 95% of the length to effectively model the structural damage [64]. Nonlinear coupled moment-axial hinges were assigned at the beam ends to represent damage at various levels of ground motion. Axial hinges were utilized for the braces. To more accurately represent the damage in non-structural components, such as pipes and tanks, shell elements were employed. This modelling approach considered the coupled nonlinear behaviour, incorporating hysteresis properties derived from a recent experimental study [65]. For the tanks, hydrostatic pressure was considered, while sloshing effects were neglected. Additionally, the compressive strain buckling behaviour of the pipes was analysed using the specified model from literature [66] which represented in Eq. (12). Shear deformation was considered in both structural and non-structural members by defining shear properties in shell elements and incorporating shear stiffness in frame elements. To accurately capture the nonlinearity of the material under cyclic loading, the Von Mises plasticity model was applied to the frame and tank elements, considering both isotropic and kinematic hardening. Where can I in this paragraph add that hydrostatic pressure of the tanks considered for tanks and the sloshing effect ignored

$$\varepsilon_{Cu} = 0.5\left(\frac{t}{D}\right) - 0.0025 + 3000\left(\frac{\sigma_h}{E}\right)^2 \tag{12}$$

where σ_h is hoop stress due to internal pressure, *t* is the thickness of the pipe and *D* is the diameter. For simplification in this study, the hoop stress was considered zero.

It was assumed that all beam-column connections were fixed, and non-structural components were linked to the primary structure using linear link elements.

Deep foundation includes piles with 16 meters in length and a diameter of 0.45 meters designed according to the soil characteristics specified to the case study location. The stiffness of the soil was modelled using nonlinear link elements connected to the piles at one-meter intervals [67]. The modelling incorporated various soil capacity curves: the p-y curve, which corresponds to the lateral behaviour of the soil; the t-z curve, representing the skin friction force; and the Q-z curve, illustrate the end-bearing capacity of the piles. 4% damping was assigned using the Rayleigh damping as recommended in [68].

To apply the effects of corrosion and ageing effect, a model as represented in Eq. (2) was utilized [48]. In this study, it was assumed that a three-layered inorganic coating, consisting of zinc, epoxy, and polyurethane, was initially applied to the steel surfaces [50]. This multi-layered coating was intended to protect the steel from potential corrosion damage. To model metal corrosion in the absence of coating layer, the methodology outlined in ISO 9223-4 was employed [34,69]. In this study the worst-case corrosion damage scenario was considered, applying uniform corrosion loss across the entire cross-section which all parts of the section experience an equal thickness reduction. Corrosion damage was applied only to structural components in this study, based on the assumption that non-structural components were adequately protected.

Table 1. Values utilized for computing corrosion loss [50,69]

Variable	Value	Unit
Corrosion rate	0.200	mm/year
Long-term coefficient	0.549	-
T_{50}	30.00	year
T_U	41.40	year
t_c	2.00	year
D(t)	1.42	mm

It was also assumed that the initial damage to the coating occurs after two years (t_c). Based on such assumption and considering the design life of the structure (1.25 × 50 = 63), the corrosion loss, *D(t)*, was calculated. Table 1 summarizes the values utilized to calculate the corrosion loss for this study.

5.2. Input ground motion records

Due to the proximity of the structure to one of the faults, both near-field and far-field seismic records were considered for the response-history analysis. 10 far-field and 10 near-field records were selected, each with magnitudes exceeding 5.5 and shear velocities ranging between 180-360 m/s for both mainshock and aftershock motions. The mainshocks were adjusted to closely align with the design spectrum within a specific period range, capturing 85% of the modal mass participation, as illustrated in Fig. 6 from the PEER ground motion database [70]. All aftershocks were selected from the same event and location as the mainshock was recorded with most obtained from the same station. Joyner-Boore distance (R_{jb}) value of under 20 kilometres considered as the criterion for selecting the near-field records. Additional information can be found in Table 9 and Fig. 15 in Appendix A.

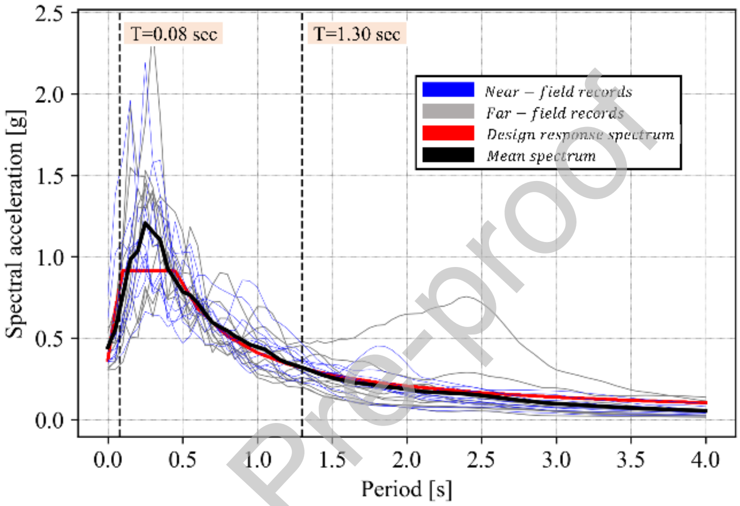

Fig. 6. Response spectra of the input ground motions and design response spectrum for the site of construction.

6. Results

6.1. Modal analysis

To investigate the impact of earthquakes on performance of the case study structure within the linear region and compute predominant frequencies, comprehensive modal analysis was performed. This type of analysis provides invaluable insights into the structural response dynamics, enabling to predict reliably the behaviour of the refinery under strong ground motions.

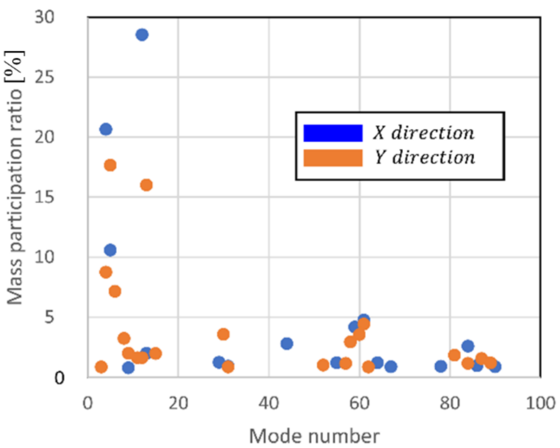

(a)

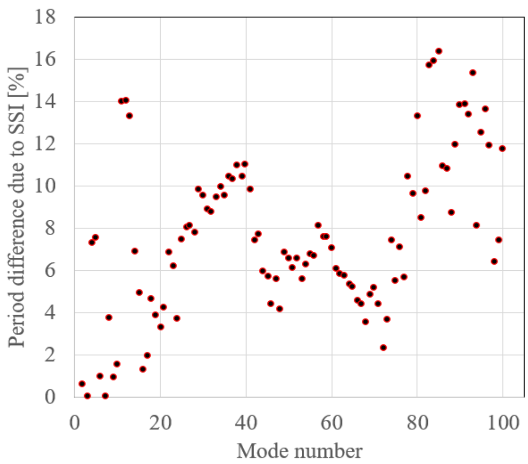

(b)

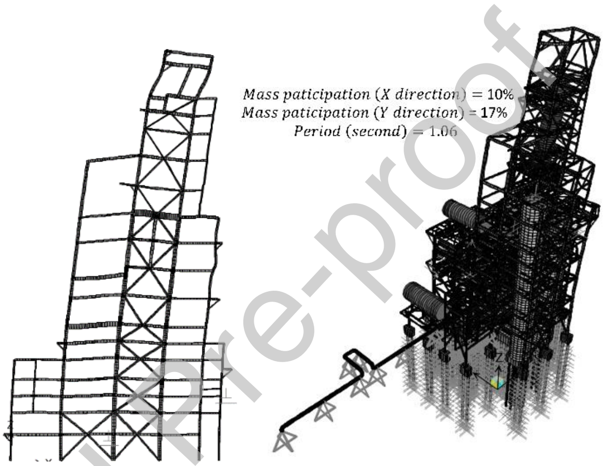

(c)

Fig. 7. Modal analysis results: (a) mass participations, (b) effect of soil-structure interaction, (c) 5th mode shape as an example

The results as illustrated in Fig. 7 and Table 2 indicate that approximately 85% of the mass participation occurred within the period range of 0.08 to 1.30 seconds. This concentration is because of the irregularity of the structure in plan and along the structure height and also the presence of reactors and vessels. Consequently, the spectral acceleration of the first mode, which is commonly employed as an intensity measure in structural analysis, contributes lower mass participation percentage and may not accurately monitor the performance of the structure during earthquake.

Table 2. Considered period range

Direction	Period range (sec)	Total mass participation (%)
X	0.08 ~ 1.19	≥ 85%
Y	0.08 ~ 1.30	

To ensure consistency between the seismic motions and the anticipated ground motions at the study location, the mainshock ground motions within the 0.08 to 1.30-second range were appropriately scaled to align with the desired design spectrum acceleration in that interval (see section 5.2).

As illustrated in Fig. 7b, soil-structure interaction (SSI) can increase the vibration period by up to 17%, with its effect varying across different modes. This difference highlights the influence of SSI on modal characteristics and structural dynamics.

6.2. Response analysis

6.2.1 Characterization of optimal intensity measure

Response analysis of a structure is typically assessed by monitoring its behaviour across various intensity measures (IMs). Appropriate deal Engineering Demand Parameter (EDP) should accurately capture the response of the structure with minimal error. To ensure the utmost accuracy in the evaluations, it is essential to identify and employ the optimal combination of EDPs and IMs.

Several studies have proposed methodologies to assess and compare the adequacy and reliability of intensity measures in predicting structural responses [71–76]. They studied the effectiveness of different IMs in predicting structural demands, reducing uncertainty in probabilistic seismic demand models, and improving fragility assessments. The primary quality to assess an IM is its dispersion which represented by the standard deviation (denoted as β in Eq. (4)). An effective IM should exhibit a lower standard deviation. Another factor is the correlation between the IM and structural demand. A desirable IM should accurately represent the relationship between changes in IM and resultant EDP. This correlation is represented by the steepness of the predicted line (coefficient 'a' in Eq.(3)) in regression analysis. Higher slope exhibits the more practical IM. Composite metric, termed the "proficiency parameter", which captures the combined influence of both dispersion and the correlation between the data. The proficiency of IM can be quantified as the ratio of its standard deviation to the slope (β/a). A lower value of this ratio indicates more reliable IMs. It is essential to consider the independence of IM from ground motion characteristics, such as magnitude (M_w) and epicentral distance (R_e). This comparison signifies the reliability of the IM when applied in Probabilistic Seismic Demand Models (PSDM), illustrating how M_w and R, given a specific IM, influence the seismic demand model. A higher p-value resulting from regression analyses between residuals and ground motion characteristics (M_w and R) shows a more reliable IM. Ultimately, the chosen IM should align well with the hazard characteristics of the study region. The importance of selecting efficient intensity measures that minimize record-to-record variability in seismic demand estimation has been highlighted [77]. Traditional IMs, such as PGA and $Sa(T_1)$, have been shown to exhibit significant dispersion, leading to uncertainty in demand predictions, particularly for nonlinear structural responses. Structure-specific IMs have also been introduced, emphasizing their role in capturing both near and far-field ground motions [78]. It has been suggested that sufficiency and efficiency should be key criteria in selecting IMs, particularly for structures where higher-mode effects are significant.

In this study, sensitivity of structural response in relation to the period, amplitude, and duration of the intensity measure (IM) was evaluated considering four different intensity measures: peak ground acceleration (PGA), spectral acceleration at the dominant modes ($Sa(T_d)$), which represents the average intensity measure within the range of dominant vibration periods, Arias intensity (AI), and cumulative absolute velocity (CAV), as shown in Table 3 & Table 4.

Table 3. Statistical characteristics of intensity measures under primary motions.

	Attribute	β/b	p-value	R^2[%]

Intensity measure		Uncorroded	Corroded	Uncorroded		Corroded		Uncorroded	Corroded
				M_w	R	M_w	R		
Sa(T_d)	Period-based	0.12	0.11	0.67	0.46	0.61	0.24	81	82
PGA	Amplitude-based	2.56	2.62	0.03	0.28	0.02	0.50	20	22
CAV	Duration-based	0.52	0.6	0.04	0.69	0.03	0.86	20	23
AI	Duration-based	0.82	1.2	0.02	0.41	0.02	0.79	21	21

Table 4. Statistical characteristic s of intensity measures under sequence motions

Intensity measure	Attribute	β/b		P-value				R^2[%]	
		Uncorroded	Corroded	Uncorroded		Corroded		Uncorroded	Corroded
				M_w	R	M_w	R		
Sa(T_d)	Period-based	0.22	0.22	0.48	0.43	0.84	0.63	54	53
PGA	Amplitude-based	0.75	0.79	0.04	0.11	0.27	0.69	20	21
CAV	Duration-based	0.34	0.46	0.18	0.85	0.48	0.96	32	20
AI	Duration-based	0.45	0.54	0.65	0.42	0.33	0.97	21	19

According to statistical results, spectral acceleration at the dominant modes (Sa(T_d)) showed the strongest correlation with data, the least dispersion, and the highest accuracy (R^2) compared to other measures of intensity. The results indicate that the structural response is significantly affected by the dominant periods that govern the performance of the petrochemical unit. While CAV demonstrated the highest p-value, indicating a good correlation with ground motion characteristics, considering the hazard curve (Fig. 4-b) and comparisons with other statistical factors suggest that it may not be the most suitable intensity measure for this case study.

6.2.2 Cloud analysis

Fig. 8a&b illustrate the cloud (regression) analysis of the data, using the maximum inter-story drift ratio (MIDR) as the response parameter to represent damage accumulation in both structural and non-structural components and Sa(T_d) of the mainshock as the optimal intensity measure to represent the severity of the input ground motion. The results are compared under mainshock records (MS) and when followed by strong aftershock (MS+AF).

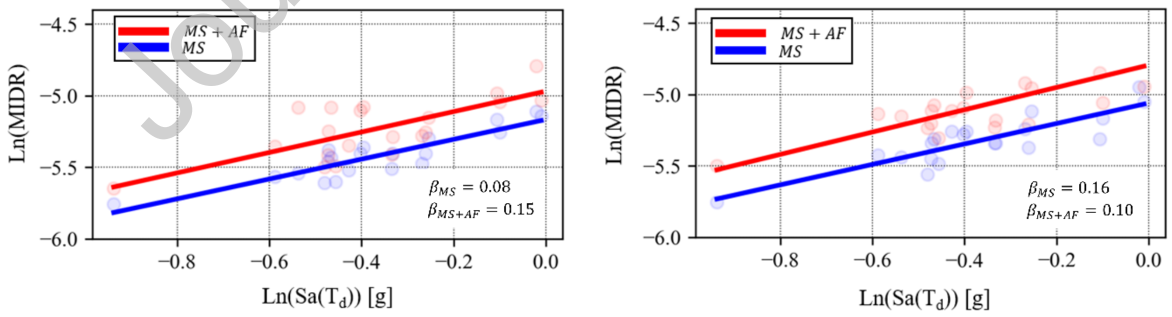

(a) (b)

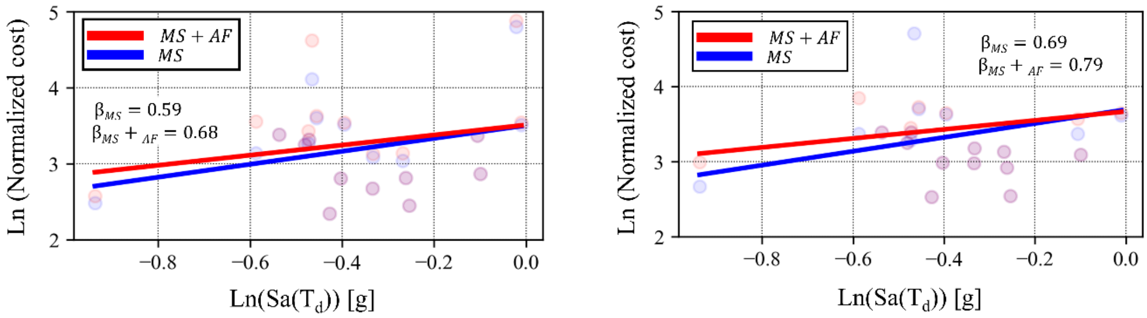

(c) (d)

Fig. 8. Cloud analysis for: (a&c) uncorroded model and (b&d) corroded model.

The results indicate that aftershock records can increase the structural response value, possibly, resulting in higher damage level. Aftershock effect was more significant in the case with ageing, i.e. when subjected to corrosion attacks. As an example, for an uncorroded model, the aftershocks can amplify the demand by up to a factor of 1.6. In contrast, for a corroded structure, this factor can reach approximately 1.8.

Fig. 8c&d represent correlation between earthquake severity and repair costs. All costs, were normalized to the repair cost associated with braces were obtained from the Federal Emergency Management Agency (FEMA-P-58) consequence estimation database [79] as illustrated in

Table 5. Based on expert opinions, it was presumed that the repair costs for beams and seamless pipes, upon reaching their yield capacity, were approximately double the repair cost associated with braces. Furthermore, the repair cost for columns was estimated to be three times this value.

Table 5. Structural consequence estimation according to FEMA P-58 [79]

NISTIR* classification	Component	Description	Damage level
B1033.052	Ordinary Concentric Braced Frame w compact braces, Single Diagonal Brace	The brace is buckled, but has not exceeded its depth. The gusset and framing show initial yielding without buckling. Residual brace deformation is minimal, and drift is slight.	Slight
B1033.052	Ordinary Concentric Braced Frame w compact braces, Single Diagonal Brace	The brace is fractured, gusset detached, framing shows local buckling, and bolt fractures are evident in beam-column connections.	Severe

NISTIR= National Institute of Standards and Technology

Due to rarity of observed yielding of reactor tanks in some cases, the repair costs for steel tanks were not considered into these calculations.

The cost analysis indicates that aftershocks might slightly increase repair costs, especially under lower seismic intensities. However, as the severity of the earthquake increases, this effect becomes less pronounced. The results can be utilized to estimate the total costs associated with the structure throughout its lifetime.

6.2.3 Damage analysis

To more accurately assess damage probability at different intensity levels, defining clear and relevant damage states is crucial. Such states should represent the varying degrees of damage a structure might undergo during an earthquake. They range from slight damage, which indicates low damage level and minimal consequences, such as approaching the first yielding capacity in structural elements or damage to non-critical facilities to extreme damage state, often referred to as the collapse prevention level which is the highest damage level the structure can experience. At this level, most structural elements reach their ultimate capacities, accompanied by leaks and ruptures in critical equipment. Table 6 illustrates these different damage states for the structure obtained using pushover analysis.

Table 6. Damage states selected for the case study

Damage state level	Performance objectives	MIDR [%]
Slight	Several braces or beams approach their yield capacity	0.28
Moderate	The first pipe reaches its yield capacity, the reactor tanks yield and a few beams and braces experience minor damage	0.51
Severe	First column reaches its yield capacity, followed by beams or braces reaching their ultimate capacity, accompanied by minor damage to several pipes	1.10
Extreme [52]	Several pipes reach their tensile or compressive ultimate capacities with tanks experiencing buckling, and structural elements severely damaged	4.70

During the pushover analysis, the structural response was monitored at each step. The results revealed that the initial damage was associated with the yielding of braces or beams within the structural elements. Damage to non-structural elements commenced with the pipes reaching their yield capacity identified as the second damage state. This particular damage level, termed as the control damage state, can be addressed through certain repair measures, ensuring the unit's full safety is reinstated. Severe damage level was considered when the first column reached its yield capacity, accompanied by a few beams and braces reaching their ultimate capacity and several pipes undergoing yielding. At this stage, the structural frame was significantly damaged, while non-structural elements exhibit moderate damage. Reaching the extreme damage level which indicate the global damage state, most structural and non-structural components experience severe damage and the risk of pipe leakage becomes notably elevated. At this step, petrochemical unit should be promptly shut down to facilitate necessary repair activities. The maximum inter-story drift ratio, as the response metric for the entire system, was determined for each damage state. During the pushover analysis, no damage was observed in the tanks. However, damage was closely monitored through multiple time history analyses. It was concluded that when the structure was subjected to near-field records, the tanks reached their yield capacity and the MIDR of the structural frame exceeded 0.40%. Conversely, no damage was observed under far-field records. The 'elephant foot' buckling damage mode, frequently observed in steel tanks, becomes apparent prior to reaching the ultimate damage state according to [52].

As the structure was designed linearly, only the initial three damages were observed during seismic events. Fig. 9 illustrates the fragility curves across various damage levels. The results indicate that aftershock motions can elevate the probability of damage at different levels. As the structure progresses to higher damage levels, it transitions into the nonlinear region and the influence of aftershocks becomes more pronounced compared to when structure behave linearly (stiffness control stage) at lower damage states. Furthermore, the effect of corrosion on the probability of damage becomes greater at higher damage levels. For example, at $Sa(T_d)=$ 2g, the probability of attaining the severe damage state (damage state 3) for the corroded structure is approximately 60% higher than that for the uncorroded case.

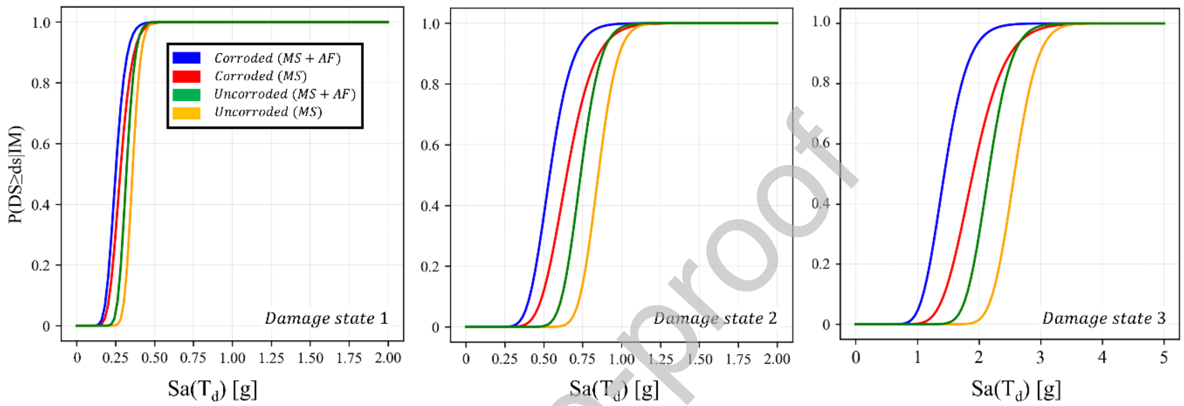

(a) (b) (c)

Fig. 9. Seismic fragility curves for (a) slight, (b) moderate and (c) severe damage states.

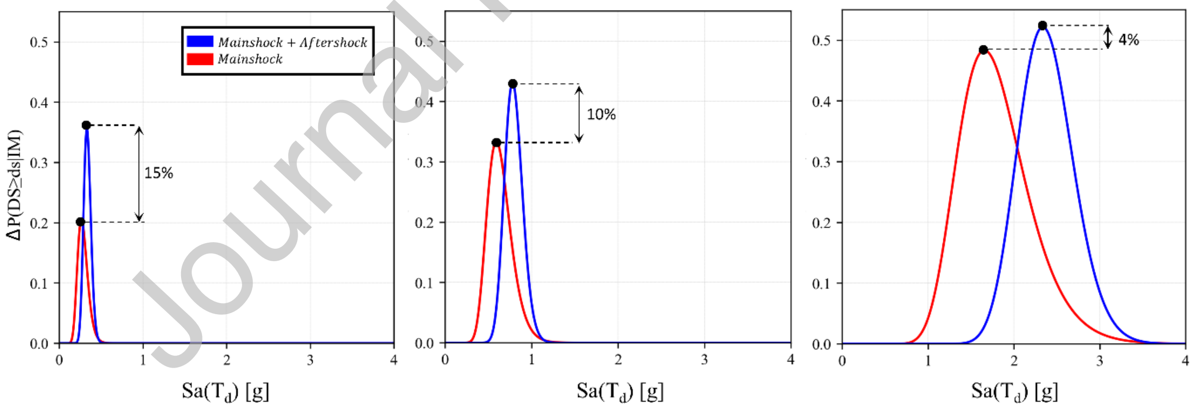

(a) (b) (f)

Fig. 10. Effect of corrosion in (a) slight, (b) moderate and (c) severe damage states.

To illustrate the influence of aftershocks on corroded structure, the differences in the probability of damages between corroded and uncorroded scenarios are plotted in Fig. 10 for various damage states. The results indicate that the impact of corrosion becomes increasingly significant as the damage state progresses. Furthermore, as structures experience more severe damage levels, the difference in peak values diminishes. For instance, in the case of slight damage, the peak value sees a rise of 75%. However, in severe damage state, this increase is approximately 30%. Additionally, corrosion influences a broader range of intensity measures in higher damage states.

To assess further the influence of aftershocks over the lifetime of the structure, the surface fragility is plotted in Fig. 11. The results indicate that the impact of aftershocks is more severe when the structure is corroded (structure exhibiting ageing effects).

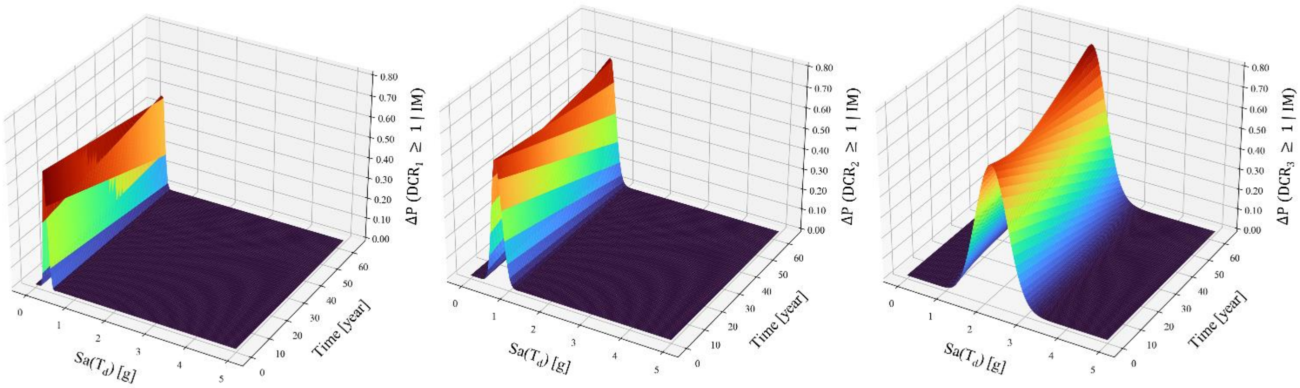

Fig. 11. The effect of aftershocks on fragility of the structure at: (a) slight, (b) moderate and (c) severe damage states

As illustrated in Fig. 11 the aftershock effect intensifies notably as the damage progress to higher levels. This effect underscores the importance of considering aftershocks in seismic risk assessments.

6.2.4 Life cycle cost analysis

To evaluate the life cycle costs (LCC) of the refinery, this paper outlines two management scenarios over the design life of the structure. The first scenario considers comprehensive corrosion management throughout the design life of the structure. On the other hand, the second scenario considers a corroded structure assumes no specific corrosion management strategies. The LCC analysis of both cases start with identical initial costs, including material costs, as well as the costs associated with the initial coating application. Additionally, anticipated repair costs attributable to seismic activities, as determined in the cost analysis presented in section 6.2.2, are included into future costs. For this study, a discount rate of 3.5% is applied [80] to represent the time value of money and evaluate the present worth of maintenance costs over the lifetime of the structure through the calculation of Net Present Value (*NPV*). The details of the LCC analysis are summarized in Table 7 and Table 8.

Table 7. Breakdown of the initial costs [50]

Initial costs	Material	Price Basis	Unit cost
Construction materials	Carbon steel Stainless steel	USD/ton	550 3,000
Initial painting (IP)	IOZ/Epoxy/Polyurethane *	USD/ sq. ft	2.587

* IOZ= Inorganic zinc

Table 8. Breakdown of maintenance costs [50]

Maintenance plan	Painting occurs in year	Price Basis	Unit cost
Touch-up	SL [a]	0.5*IP*RF [b]	0.746
Maintenance re-paint	1.5*SL	0.9*IP*RF	1.020

[a] SL= Coating service life; [b] RF= Reduction factor.

The unit costs for materials, including carbon steel (used for supporting structures and steel tanks) and stainless steel (employed for steel pipes), have been determined through market research and referencing prior studies conducted in the year the asset was constructed [81]. The unit cost for corrosion-resistant coatings has been determined, considering a service life of the coating layer of 16 years. This assessment includes the costs related to surface preparation, initial paint materials, and the costs for applying the three coating layers, including labour fees.

Two key checkpoints can be considered for the corrosion maintenance plan throughout the design life of the refinery. The first involves touch-up painting at the end of the coating layer's service life (SL), while the second entails repainting areas where the paint has been removed after reaching 1.5 times the service life of the coating layer.

The results of the LCC analysis are illustrated in Fig. 12. All costs have been normalized to the initial cost presented in the case study.

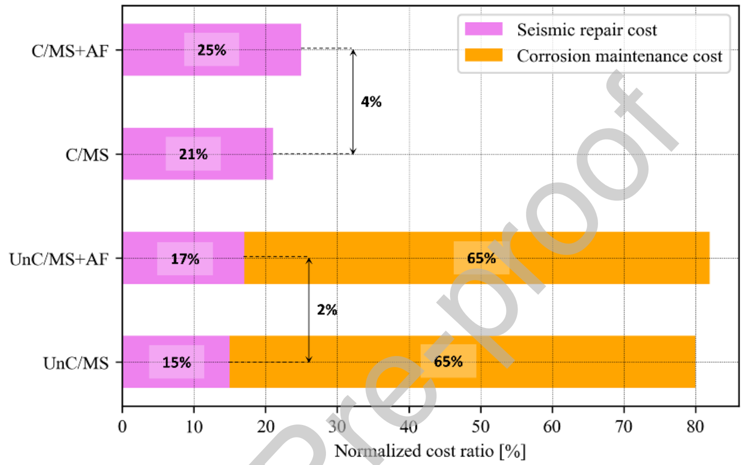

Fig. 12. Life cycle cost analysis for uncorroded (UnC) and corroded (C) structures under mainshocks (MS) and aftershocks (AF).

The results revealed that corrosion maintenance costs accounted for the most significant ratio, comprising 65% of the total initial cost of project. The seismic repair costs for the corroded structure (no maintenance plan) increased by 6% during mainshocks and 8% during aftershocks compared to an uncorroded structure (with maintenance plan). This underscores the substantial effect of corrosion on the projected repair costs for the structure. For uncorroded and corroded structures, a 2% and 4% increase in repair costs was observed during aftershocks, respectively. This highlights the effect of aftershocks on the repair costs.

The overall LCC ratio was approximately 80% for the uncorroded scenario without maintenance, whereas it reduced to around 20% for the corroded structure over the design life of the case study. Nevertheless, employing alternative maintenance strategies, or increased corrosion-induced deterioration could potentially alter these ratios.

7. Risk assessment

For facilitating the decision-making process, risk metrics were utilized, which combined the hazard characteristics of the study region with the probability of damage occurrence (fragility function). Fig. 13 illustrates the annual failure rates of each damage states.

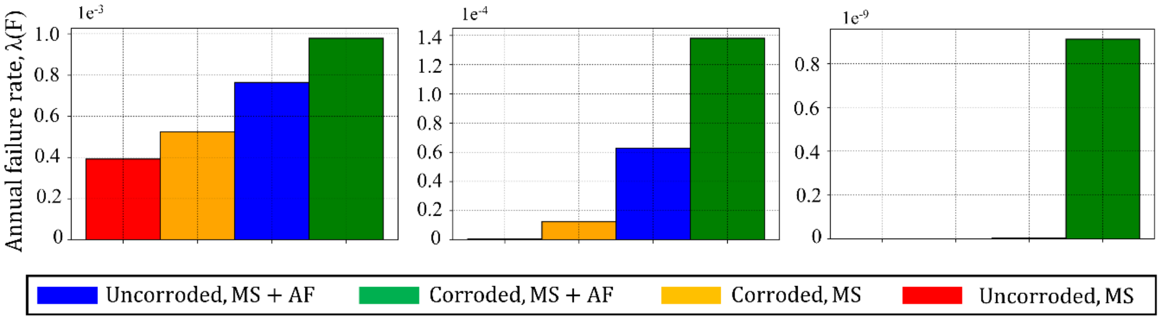

(a) (b) (c)

Fig. 13. Annual failure rate at: (a) slight, (b) moderate and (c) severe damage state

The results indicate that both aftershock motions and corrosion contribute to a higher risk of damage in the refinery unit. The most significant risk was observed in the corroded structure at its design life, when subjected to earthquake sequence. For the first damage state, the annual failure rate was approximately 0.001 (1/year) for corroded structure, corresponding to a return period of 1,000 years. However, for the second damage state, the return period was roughly 7 times longer than the this value. In case of uncorroded refinery unit, the return period was approximately 13 times longer for the second damage state compared to the first when exposed to the earthquake sequence.

The effect of aftershock motions on the first damage state was approximately twice as pronounced in the case of the uncorroded model. Similarly, this factor was also the same for the corroded model. Based on the hazard characteristics of the study region, it can be determined that the risk for the uncorroded structure to incur more than slight damage is nearly zero. These results emphasize the compounded risks associated by both corrosion and seismic sequence on the structural integrity of the case study.

Fig. 14 illustrates the relative recovery time and resilience of the petrochemical unit after experiencing ground motion records. Based on engineering judgment and web research, it is concluded that braces may be easier to inspect, repair, or replace due to their accessibility. Beams, due to their larger size and the complexity of their connections, require more detailed inspections to assess damage, thus necessitating more recovery time. Columns, as critical load-bearing elements, require careful repair to ensure the building's structural integrity, leading to even longer recovery times than beams. Non-structural components, such as steel pipes, are expected to have shorter recovery times than braces due to better accessibility and the feasibility of replacement. Assuming that steel reactor tanks are to be replaced rather than repaired, the replacement process is considered to have the longest recovery time in this study due to the extensive timing for removal of the damaged tank and the consideration of installation time.

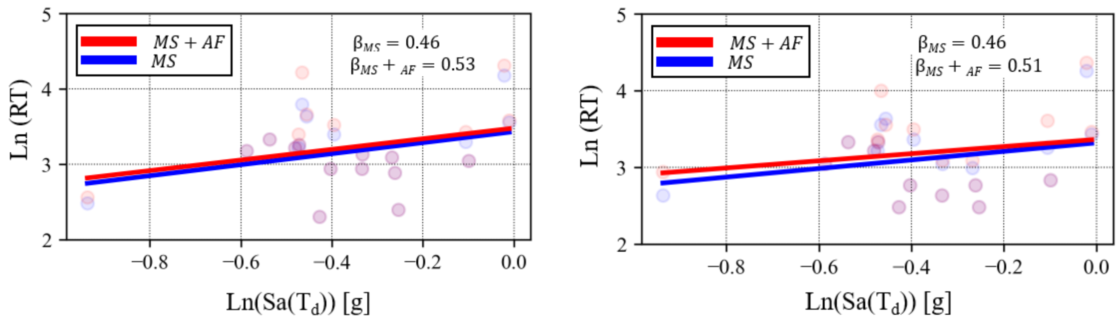

(a) (b)

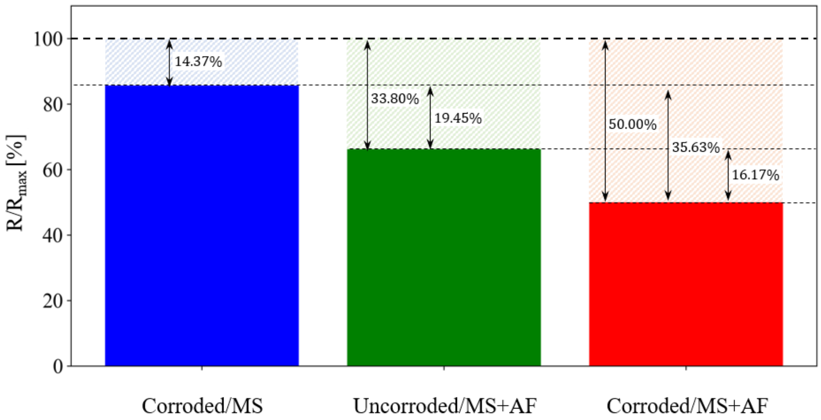

(c)

Fig. 14. Regression analyses of seismic recovery times for (a) uncorroded and (b) corroded unit, with (c) a comparison of normalized resilience.

Fig. 14-a&b display the linear regression analysis of the normalized recovery time (relative to the minimum recovery time) against the intensity of each ground motion, considering both mainshock and subsequent motion sequences. It is observed that recovery times increase as the intensity of the ground motion rises. Additionally, aftershocks slightly influence the results, with a more pronounced effect observed in corroded systems. Fig. 14-c illustrates the resilience factor normalized to the resilience of the uncorroded model (R_{max}). The results indicate that corrosion can reduce resilience by approximately 14% under main shock motions (MS), and this reduction can escalate to about 50% when considering the combined effect of mainshock and aftershocks (MS+AF). The presence of aftershocks can further reduce resilience by 16.17% in structures experiencing aging effects.

8. Conclusions

In this study, the seismic risk evaluation of an operational refinery unit was determined using probabilistic methods incorporating aging effects and aftershocks. Nonlinear time history analyses were performed to estimate the responses of the unit to strong seismic motions. The results underscore the combined vulnerabilities arising from both corrosion and seismic activities on refinery unit structures. Major results from the study are summarized as follows:

1. Structural elements within the petrochemical unit experience more severe damage compared to non-structural components. Additionally, the occurrence of corrosion, coupled with the effects of aftershock motions, amplifies the frequency of failures. With an increase in damage severity, the effects of both aftershocks and corrosion on seismic risk escalate.
2. Near-field seismic records have a greater impact on non-structural performance than far-field records, with steel reactor tanks particularly sensitive to near-field motions.
3. At severe damage level, the impact of corrosion on probability of damage is nearly identical, whether it experiences the mainshock or aftershocks with a difference of approximately 4%. However, in low damaged states, this effect becomes notably more significant, being 15% higher when the structure experiences aftershocks. As the damage level increase, the influence of corrosion extends to a broader spectrum of intensities.

4. Corroded unit under sequence motions experiences the highest risk of failure at slight damage level, with an estimated return period of 1,000 years.
5. Both corroded and uncorroded structures when subjected to sequence motions demonstrate an identical annual rate of slight damage. This rate is approximately twice as much when the structure only affected by mainshocks.
6. Structures subjected to mainshock events exhibited negligible risk of severe damage. However, there is a slight risk of damage when aftershocks occur.
7. Lack of maintenance planning coupled with the effect of aftershocks can slightly increase the life cycle costs of the structure. The costs may rise by 2% and 4% for uncorroded and corroded structures, respectively, due to aftershocks.
8. Corrosion significantly reduces structural resilience, and this reduction is heightened by the occurrence of aftershocks. Aftershocks contribute to an extra 2% decrease in resilience for structures that are already corroded, emphasizing their increased risk during seismic events.

The results emphasize the need for refinery design improvements that account for aging effects and multiple earthquakes. For facilities located in regions prone to earthquake swarms, resilience strategies should incorporate multi-event seismic demand assessments, robust structural reinforcement, and adaptive maintenance planning.

Additional investigations are required in future studies regarding the influence of pressure and sloshing in steel pipes and tanks, corrosion effects on pipes and sensitivity of other engineering demand parameters to seismic excitations. Further research is needed to investigate the effects of climate change, non-uniform corrosion types such as pitting corrosion, and the adoption of more realistic corrosion modelling approaches for accurately evaluating the long-term performance of existing refinery units. Moreover, identifying the optimal intensity-demand relationship and implementing hazard-consistent ground motion selection methods, including conditional spectra for mainshock–aftershock sequences, remain important directions for future work. Developing improved methods for combining seismic demands, accounting for residual deformations, damage accumulation, and structural degradation, is essential.

Appendix A.
Summary of input ground motions

Input ground motion obtained from PEER database [70] is presented in Table 9.

Table 9. Properties of the ground motion records based on PEER database

#	Mainshock records					Aftershock records					PGA
	RSN	M_w	R_{jb} (km)	V_{s30} (m/s)	PGA (g)	RSN	M_w	R_{jb} (km)	V_{s30} (m/s)	PGA (g)	(MS/AF)
1*	176	6.53	21.98	249.92	0.14	194	5.01	23.76	237.33	0.07	2.00
2	945	6.69	37.67	349.6	0.06	1675	5.93	51.41	349.6	0.01	6.00
3	971	6.69	36.2	326.19	0.15	1654	6.05	38.82	326.19	0.02	7.50
4	122	6.50	33.32	249.28	0.10	131	5.91	41.37	249.28	0.02	5.00
5	1748	5.90	12.62	240.09	0.29	1750	5.93	37.26	240.09	0.16	1.81
6	968	6.69	43.2	271.9	0.24	1653	6.05	42.8	271.9	0.05	4.80
7	287	6.90	44.62	356.39	0.05	298	6.2	43.5	356.39	0.03	1.67
8	7	6.60	91.15	219.31	0.06	8	6.4	44.52	219.31	0.14	0.43
9	604	5.99	45.98	267.49	0.14	3694	5.27	47.89	267.49	0.03	4.67
10*	4474	6.30	49.21	356.39	0.04	4515	5.6	87.47	310.01	0.08	0.50

11	949	6.69	3.30	297.71	0.37	1651	6.05	1.48	297.71	0.11	3.36
12	988	6.69	15.53	277.98	0.26	1658	6.05	18.34	277.98	0.11	2.36
13	162	6.53	10.45	231.23	0.29	195	5.01	11.17	231.23	0.11	2.64
14	214	5.80	15.19	377.51	0.16	223	5.42	14.31	377.15	0.28	0.57
15	4349	6.00	0.80	317.00	0.21	4385	5.60	10.50	317.00	0.10	2.10
16	174	6.53	12.56	196.25	0.48	199	5.01	13.61	196.25	0.10	4.80
17	1	6.00	2.07	593.35	0.17	2	6.00	2.09	551.82	0.05	3.40
18	231	6.06	12.56	537.16	0.46	250	5.94	9.65	537.16	1.02	0.45
19	1039	6.69	16.92	341.58	0.33	1681	5.93	13.61	341.58	0.19	0.62
20	368	6.36	7.69	257.38	0.61	412	5.77	13.16	257.38	0.58	0.45

* Mainshock and aftershock records are from different stations due to a lack of data

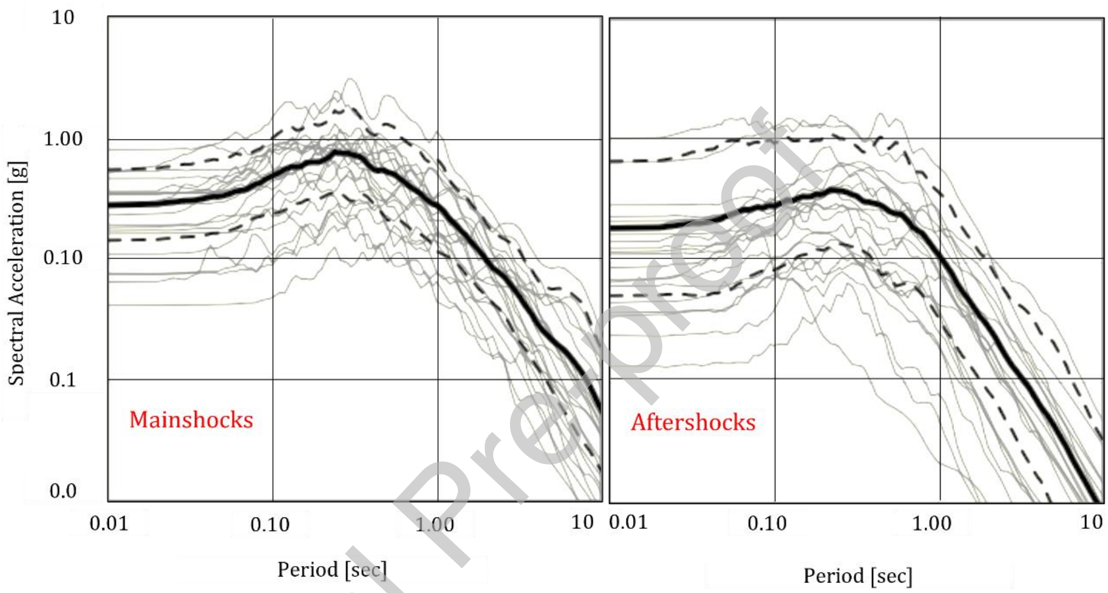

Fig. 15. Response spectral acceleration of the selected ground motion records

Appendix B.

List of abbreviations and symbols

MIDR	=	Maximum Inter-story Drift Ratio
IM	=	Intensity measure
EDP	=	Engineering demand parameter
$Sa(T_d)$	=	Spectral acceleration at the dominant modes
CAV	=	Cumulative absolute velocity
AI	=	Arias intensity
M_w	=	Magnitude of earthquake
R	=	Resilience index
R_e	=	Epicentral distance
R_{jb}	=	Joyner-Boore distance
β	=	standard deviation (dispersions)
R^2	=	Coefficient of determination
a	=	Slope of the predicted line

MS	=	Mainshock record
MS+AF	=	Mainshock-aftershock record
DCR	=	Demand to capacity ratio
λ	=	Annual failure rate

Acknowledgements

The industrial PhD project titled "Monitoring of Ageing Steel Bridges for Lifetime Extension and Resilience Enhancement" (MOST-RESILIENT) received financial funding from the Low Carbon Eco-Innovatory Research Programme (LCEI) via the European Regional Development Fund (ERDF) at the University of Liverpool. Views, opinions, findings, and conclusions articulated in the manuscript are those of the authors and do not necessarily represent the perspectives of the funding bodies.

Authorship Contributions

Luigi Di Sarno: Conceptualization, Writing and Revision; Armin Majidian: Writing, Numerical Analyses and Conceptualization.

Ethical Approval

The content contained within this analytical work does comply with Ethical rules and is also according to the principles of Gender and Inclusion.

Funding details (In case of Funding)

There is no specific funding. Further details in the acknowledgements.

Conflict of Interest

There is no conflict of interest for the submission of this manuscript.

Informed Consent

All authors and parties mentioned in the paper are aware and do agree with the contents presented.

References

[1] Casal J. Evaluation of the effects and consequences of major accidents in industrial plants, Elsevier. 2017.
[2] Casal J. Evaluation of the Effects and Consequences of Major Accidents in Industrial Plants, Elsevier; 2018, p. 1–24. https://doi.org/10.1016/b978-0-444-63883-0.00001-0.
[3] European Commission, Natural Hazard-Triggered Technological Accidents Database (Natech) n.d. https://enatech.jrc.ec.europa.eu/ (accessed December 11, 2023).
[4] European Commission, The Major Accident Reporting System (MARS) n.d. https://emars.jrc.ec.europa.eu/ (accessed December 11, 2023).
[5] Ricci F, Casson Moreno V, Cozzani V. A comprehensive analysis of the occurrence of Natech events in the process industry. Process Safety and Environmental Protection 2021;147:703–13. https://doi.org/10.1016/J.PSEP.2020.12.031.
[6] EM-DAT CR, The international disasters database, Center for Research on the Epidemiology of Disasters. Disponivel em. https://www. emdat. be. n.d.

[7] Krausmann E, Cruz AM. Impact of the 11 March 2011, Great East Japan earthquake and tsunami on the chemical industry. Natural Hazards 2013;67:811–28. https://doi.org/10.1007/S11069-013-0607-0/FIGURES/8.

[8] Sezen H, Whittaker AS. Seismic Performance of Industrial Facilities Affected by the 1999 Turkey Earthquake. Journal of Performance of Constructed Facilities 2006;20:28–36. https://doi.org/10.1061/(ASCE)0887-3828(2006)20:1(28)/ASSET/FC01BE9E-B889-4B59-8E2B-1D7BB1DDDFAC/ASSETS/IMAGES/11.JPG.

[9] Krausmann E, Cruz AM, Affeltranger B. The impact of the 12 May 2008 Wenchuan earthquake on industrial facilities. J Loss Prev Process Ind 2010;23:242–8. https://doi.org/10.1016/J.JLP.2009.10.004.

[10] Koch GH, Brongers MPH, Thompson NG, Virmani YP, Payer JH, CC Technologies Inc, et al. Corrosion Cost and Preventive Strategies in the United States [Final report] 2002. https://doi.org/10.21949/1503647.

[11] Al-Moubaraki AH, Obot IB. Corrosion challenges in petroleum refinery operations: Sources, mechanisms, mitigation, and future outlook. Journal of Saudi Chemical Society 2021;25:101370. https://doi.org/10.1016/J.JSCS.2021.101370.

[12] Speight JG. Oil and Gas Corrosion Prevention: From Surface Facilities to Refineries. Oil and Gas Corrosion Prevention: From Surface Facilities to Refineries 2014:1–151. https://doi.org/10.1016/C2013-0-18548-0.

[13] Merino Vela RJ, Brunesi E, Nascimbene R. Seismic assessment of an industrial frame-tank system: development of fragility functions. Bulletin of Earthquake Engineering 2019;17:2569–602. https://doi.org/10.1007/S10518-018-00548-2/TABLES/7.

[14] Fiore A, Rago C, Vanzi I, Greco R, Briseghella B. Seismic behavior of a low-rise horizontal cylindrical tank. International Journal of Advanced Structural Engineering 2018;10:143–52. https://doi.org/10.1007/S40091-018-0188-Y/TABLES/8.

[15] Bakalis K, Karamanos SA. Uplift mechanics of unanchored liquid storage tanks subjected to lateral earthquake loading. Thin-Walled Structures 2021;158:107145. https://doi.org/10.1016/J.TWS.2020.107145.

[16] Kazantzi AK, Karaferis ND, Melissianos VE, Bakalis K, Vamvatsikos D. Seismic fragility assessment of building-type structures in oil refineries. Bulletin of Earthquake Engineering 2022;20:6853–76. https://doi.org/10.1007/S10518-022-01476-Y/TABLES/9.

[17] Karaferis ND, Kazantzi AK, Melissianos VE, Bakalis K, Vamvatsikos D. Seismic fragility assessment of high-rise stacks in oil refineries. Bulletin of Earthquake Engineering 2022;20:6877–900. https://doi.org/10.1007/S10518-022-01472-2/FIGURES/11.

[18] Di-Sarno L, Majidian · Armin. Seismic risk of typical ageing petrochemical steel structure in harsh atmospheric conditions. Bulletin of Earthquake Engineering 2023 2023:1–27. https://doi.org/10.1007/S10518-023-01702-1.

[19] Di Sarno L, Karagiannakis G. On the seismic fragility of pipe rack—piping systems considering soil–structure interaction. Bulletin of Earthquake Engineering 2020;18:2723–57. https://doi.org/10.1007/S10518-020-00797-0/TABLES/12.

[20] Zuluaga Mayorga S, Sánchez-Silva M, Ramírez Olivar OJ, Muñoz Giraldo F. Development of parametric fragility curves for storage tanks: A Natech approach. Reliab Eng Syst Saf 2019;189:1–10. https://doi.org/10.1016/J.RESS.2019.04.008.

[21] Butenweg C, Bursi OS, Paolacci F, Marinković M, Lanese I, Nardin C, et al. Seismic performance of an industrial multi-storey frame structure with process equipment subjected to shake table testing. Eng Struct 2021;243:112681. https://doi.org/10.1016/J.ENGSTRUCT.2021.112681.

[22] Melissianos VE, Karaferis ND, Bakalis K, Kazantzi AK, Vamvatsikos D. Hazard, exposure, fragility, and damage state homogenization of a virtual oil refinery testbed for seismic risk assessment. Earthquake Spectra 2025;41:547–78. https://doi.org/10.1177/87552930241272521.
[23] Di-Sarno L, Majidian A. Risk assessment of a typical petrochemical plant with ageing effects subjected to seismic sequences. Eng Struct 2024;310:118110. https://doi.org/10.1016/J.ENGSTRUCT.2024.118110.
[24] GG Deierlein HK. A framework for performance-based earthquake engineering. Proceedings of 2003 Pacific Conference on Earthquake Engineering, Christchurch, New Zealand n.d.:1–8. https://scholar.google.com/scholar_lookup?title=A framework for performance-based earthquake engineering&author=G.G. Deierlein&publication_year=2003 (accessed February 24, 2025).
[25] Du A, Wang X, Xie Y, Dong Y. Regional seismic risk and resilience assessment: Methodological development, applicability, and future research needs – An earthquake engineering perspective. Reliab Eng Syst Saf 2023;233:109104. https://doi.org/10.1016/J.RESS.2023.109104.
[26] Valente M, Ricci F, Cozzani V. A systematic review of Resilience Engineering applications to Natech accidents in the chemical and process industry. Reliab Eng Syst Saf 2025;255:110670. https://doi.org/10.1016/J.RESS.2024.110670.
[27] Cimellaro GP, Reinhorn AM, Bruneau M. Seismic resilience of a hospital system. Structure and Infrastructure Engineering 2010;6:127–44. https://doi.org/10.1080/15732470802663847.
[28] Tsionis Georgios. Seismic resilience : concept, metrics and integration with other hazards 2014.
[29] Xu G, Guo T, Li A, Zhang H, Wang K, Xu J, et al. Seismic resilience enhancement for building structures: A comprehensive review and outlook. Structures 2024;59:105738. https://doi.org/10.1016/J.ISTRUC.2023.105738.
[30] Quinci G, Paolacci F, Fragiadakis M, Bursi OS. A machine learning framework for seismic risk assessment of industrial equipment 2024. https://doi.org/10.1016/j.ress.2024.110606.
[31] Wood, M. H., Arellano, A. V., & Van Wijk, L. (2013). Corrosion related accidents in petroleum refineries. European Commission Joint Research Centre, report no. EUR, 26331. 2013.
[32] Akpanyung K V., Loto RT, Fajobi MA. An Overview of Ammonium Chloride (NH4Cl) Corrosion in the Refining Unit. J Phys Conf Ser 2019;1378:022089. https://doi.org/10.1088/1742-6596/1378/2/022089.
[33] Karagiannakis G, Di Sarno L, Necci A, Krausmann E. Seismic risk assessment of supporting structures and process piping for accident prevention in chemical facilities. International Journal of Disaster Risk Reduction 2022;69:102748. https://doi.org/10.1016/J.IJDRR.2021.102748.
[34] ISO - ISO 9223:2012 - Corrosion of metals and alloys — Corrosivity of atmospheres — Classification, determination and estimation n.d. https://www.iso.org/standard/53499.html (accessed June 28, 2022).
[35] Nguyen MN, Wang X, Leicester RH. An assessment of climate change effects on atmospheric corrosion rates of steel structures. Corrosion Engineering, Science and Technology 2013;48:359–69. https://doi.org/10.1179/1743278213Y.0000000087.
[36] Sousa ML, Dimova S, Athanasopoulou A, Dyngeland T, Pinto A, Rianna G, et al. Expected implications of climate change on the corrosion of structures n.d. https://doi.org/10.2760/05229.

[37] Zhang Y, Ayyub BM, Fung JF. Projections of corrosion and deterioration of infrastructure in United States coasts under a changing climate. Resilient Cities and Structures 2022;1:98–109. https://doi.org/10.1016/J.RCNS.2022.04.004.
[38] Di Sarno L, Majidian A, Karagiannakis G. The Effect of Atmospheric Corrosion on Steel Structures: A State-of-the-Art and Case-Study. Buildings 2021, Vol 11, Page 571 2021;11:571. https://doi.org/10.3390/BUILDINGS11120571.
[39] Rizzo F, Di Lorenzo G, Formisano A, Landolfo R. Time-Dependent Corrosion Wastage Model for Wrought Iron Structures. Journal of Materials in Civil Engineering 2019;31:04019165. https://doi.org/10.1061/(ASCE)MT.1943-5533.0002710.
[40] Landolfo R, Cascini L, Portioli F. Modeling of Metal Structure Corrosion Damage: A State of the Art Report. Sustainability 2010, Vol 2, Pages 2163-2175 2010;2:2163–75. https://doi.org/10.3390/SU2072163.
[41] Feliu S, Morcillo M, Feliu S. The prediction of atmospheric corrosion from meteorological and pollution parameters—II. Long-term forecasts. Corros Sci 1993;34:415–22. https://doi.org/10.1016/0010-938X(93)90113-U.
[42] Melchers RE. Corrosion uncertainty modelling for steel structures. J Constr Steel Res 1999;52:3–19. https://doi.org/10.1016/S0143-974X(99)00010-3.
[43] Albrecht P, Hall TT. Atmospheric Corrosion Resistance of Structural Steels. Journal of Materials in Civil Engineering 2003;15:2–24. https://doi.org/10.1061/(ASCE)0899-1561(2003)15:1(2).
[44] Klinesmith DE, McCuen RH, Albrecht P. Effect of Environmental Conditions on Corrosion Rates. Journal of Materials in Civil Engineering 2007;19:121–9. https://doi.org/10.1061/(ASCE)0899-1561(2007)19:2(121).
[45] Han X, Frangopol DM. Impact of Climate Change on Risk Assessment and Effective Maintenance Strategies for Bridge Networks Subjected to Corrosion. ASCE ASME J Risk Uncertain Eng Syst A Civ Eng 2024;10:04023054. https://doi.org/10.1061/AJRUA6.RUENG-1059/ASSET/8BB9246A-EBF9-42F3-85F9-171039632AAD/ASSETS/IMAGES/LARGE/FIGURE10.JPG.
[46] Tran NL, Nguyen TH, Phan VT, Nguyen DD. A Machine Learning-Based Model for Predicting Atmospheric Corrosion Rate of Carbon Steel. Advances in Materials Science and Engineering 2021;2021. https://doi.org/10.1155/2021/6967550.
[47] Aghaaminiha M, Mehrani R, Colahan M, Brown B, Singer M, Nesic S, et al. Machine learning modeling of time-dependent corrosion rates of carbon steel in presence of corrosion inhibitors. Corros Sci 2021;193:109904. https://doi.org/10.1016/J.CORSCI.2021.109904.
[48] Kere KJ, Asce SM, Huang Q, Asce M. Life-Cycle Cost Comparison of Corrosion Management Strategies for Steel Bridges. Journal of Bridge Engineering 2019;24:04019007. https://doi.org/10.1061/(ASCE)BE.1943-5592.0001361.
[49] Kallias AN, Imam B, Chryssanthopoulos MK. Performance profiles of metallic bridges subject to coating degradation and atmospheric corrosion. Https://DoiOrg/101080/1573247920161164726 2016;13:440–53. https://doi.org/10.1080/15732479.2016.1164726.
[50] Helsel, J. L., R. Lanterman and KW. Expected service life and cost considerations for maintenance and new construction protec- tive coating work. In Vol 4 of Proc, Corrosion Conf Expo,2438– 2459 Houston, TX:NACE International 2008.
[51] Saed G, Balomenos GP. Fragility framework for corroded steel moment-resisting frame buildings subjected to mainshock-aftershock sequences. Soil Dynamics and Earthquake Engineering 2023;171:107975. https://doi.org/10.1016/J.SOILDYN.2023.107975.

[52] Di-Sarno L, Majidian · Armin. Seismic risk of typical ageing petrochemical steel structure in harsh atmospheric conditions. Bulletin of Earthquake Engineering 2023 2023:1–27. https://doi.org/10.1007/S10518-023-01702-1.
[53] Miano A, Jalayer F, Ebrahimian H, Prota A. Cloud to IDA: Efficient fragility assessment with limited scaling. Earthq Eng Struct Dyn 2018;47:1124–47. https://doi.org/10.1002/EQE.3009.
[54] Cimellaro GP, Reinhorn AM, Bruneau M. Framework for analytical quantification of disaster resilience. Eng Struct 2010;32:3639–49. https://doi.org/10.1016/J.ENGSTRUCT.2010.08.008.
[55] Bruneau M, Eeri) M, Chang SE, Eguchi RT, Lee GC, O'rourke TD, et al. A Framework to Quantitatively Assess and Enhance the Seismic Resilience of Communities 2003. https://doi.org/10.1193/1.1623497.
[56] ISO 15686-1:2011 - Buildings and constructed assets — Service life planning — Part 1: General principles and framework n.d. https://www.iso.org/standard/45798.html (accessed January 9, 2024).
[57] ASTM, D. A36/A36M Standard Specification for Carbon Structural Steel. or A992/A992M-06A, Grade 50–Standard Specification for Structural Steel Shapes 2014.
[58] The UWI Seismic Research Centre n.d. https://uwiseismic.com/ (accessed December 25, 2022).
[59] Bozzoni F, Corigliano M, Lai CG, Salazar W, Scandella L, Zuccolo E, et al. Probabilistic Seismic Hazard Assessment at the Eastern Caribbean Islands. Bulletin of the Seismological Society of America 2011;101:2499–521. https://doi.org/10.1785/0120100208.
[60] The Weather Year Round Anywhere on Earth - Weather Spark n.d. https://weatherspark.com/ (accessed February 4, 2024).
[61] Engineering Director Inc (EDI), ISO 9223 tool n.d. https://www.engineeringdirector.com/iso9223-c1-x (accessed August 22, 2024).
[62] Trinidad and Tobago - Mean Projections | Climate Change Knowledge Portal n.d. https://climateknowledgeportal.worldbank.org/country/trinidad-and-tobago/climate-data-projections-general (accessed February 4, 2024).
[63] SAP2000 C.S.I., Structural analysis program. Berkeley, California. 2023. n.d.
[64] NIST. Recommended modeling parameters and acceptance criteria for nonlinear analysis in support of seismic evaluation, retrofit, and design. National Institute of Standards and Technology 2017:597.
[65] Karvelas C, Chatzopoulou G, Zervaki AD, Stathas N, Strepelias E, Palios X, et al. Mechanical Response of an Industrial Piping System Under Strong Cyclic Loading. American Society of Mechanical Engineers, Pressure Vessels and Piping Division (Publication) PVP 2021;5. https://doi.org/10.1115/PVP2021-62273.
[66] Vathi M, Karamanos SA, Kapogiannis IA, Spiliopoulos K V. Performance Criteria for Liquid Storage Tanks and Piping Systems Subjected to Seismic Loading. Journal of Pressure Vessel Technology, Transactions of the ASME 2017;139. https://doi.org/10.1115/1.4036916/473349.
[67] API Recommended Practice 2A-WSD Planning, Designing, and Constructing Fixed Offshore Platforms-Working Stress Design n.d.
[68] US nuclear regulatory commission D values for seismic design of nuclear power plants. Regulatory guide 2009:1–21.
[69] ISO - ISO 9224:2012 - Corrosion of metals and alloys — Corrosivity of atmospheres — Guiding values for the corrosivity categories n.d. https://www.iso.org/standard/53500.html (accessed June 28, 2022).
[70] PEER Ground Motion Database - PEER Center n.d. https://ngawest2.berkeley.edu/.

[71] Giovenale P, Cornell A, Esteva L, Giovenale P, Cornell CA, Esteva L. Comparing the adequacy of alternative ground motion intensity measures for the estimation of structural responses. Earthq Eng Struct Dyn 2004;33:951–79. https://doi.org/10.1002/EQE.386.
[72] Padgett JE, Nielson BG, Desroches R, Padgett JE, Nielson BG, Desroches R. Selection of optimal intensity measures in probabilistic seismic demand models of highway bridge portfolios. Earthq Eng Struct Dyn 2008;37:711–25. https://doi.org/10.1002/EQE.782.
[73] Karaferis ND, Kazantzi AK, Melissianos VE, Bakalis K, Vamvatsikos D. Seismic fragility assessment of high-rise stacks in oil refineries. Bulletin of Earthquake Engineering 2022;20:6877–900. https://doi.org/10.1007/S10518-022-01472-2/FIGURES/11.
[74] Bakalis K, Kohrangi M, Vamvatsikos D. Seismic intensity measures for above-ground liquid storage tanks. Earthq Eng Struct Dyn 2018;47:1844–63. https://doi.org/10.1002/EQE.3043.
[75] Feng R, Dong Y, Ye A, Wang X. Average spectral acceleration (AvgSa) for high-confidence probabilistic seismic demand modeling of urban highway bridge portfolios: What period range and damping ratio shall we use? Eng Struct 2024;309:118063. https://doi.org/10.1016/J.ENGSTRUCT.2024.118063.
[76] Khosravikia F, Clayton P. Updated evaluation metrics for optimal intensity measure selection in probabilistic seismic demand models. Eng Struct 2020;202:109899. https://doi.org/10.1016/J.ENGSTRUCT.2019.109899.
[77] Vamvatsikos D, Cornell CA. Developing efficient scalar and vector intensity measures for IDA capacity estimation by incorporating elastic spectral shape information. Earthq Eng Struct Dyn 2005;34:1573–600. https://doi.org/10.1002/EQE.496.
[78] Luco N, Cornell A, Eeri M. Structure-Specific Scalar Intensity Measures for Near-Source and Ordinary Earthquake Ground Motions n.d.
[79] Mahoney M, Hanson RD. Seismic Performance Assessment of Buildings Volume 1-Methodology Second Edition Prepared for FEDERAL EMERGENCY MANAGEMENT AGENCY n.d.
[80] Britain G. The Green Book: Appraisal and Evaluation in Central Government, Treasury Guidance. London: Her Majesty's Stationary Office 2003.
[81] Gardner L, Cruise RB, Sok CP, Krishnan K, Dos Santos JM. Life-cycle costing of metallic structures. Proceedings of the Institution of Civil Engineers: Engineering Sustainability 2007;160:167–77. https://doi.org/10.1680/ENSU.2007.160.4.167/ASSET/IMAGES/SMALL/ENSU160-167-F16.GIF.

Author Statement

We declare that this manuscript is original, has not been published before, and is not currently under consideration for publication elsewhere.

We confirm that the manuscript has been read and approved by all named authors, and there are no other individuals who meet the authorship criteria but are not listed. The order of authors has been mutually agreed upon by all contributors.

Authorship Contributions

- **Luigi Di Sarno**: Conceptualization, Writing, and Revision.
- **Armin Majidian**: Writing, Numerical Analyses, and Conceptualization.

Ethical Approval

This research complies with ethical standards and aligns with principles of gender equality and inclusion.

Conflict of Interest

The authors declare no conflicts of interest regarding the submission of this manuscript.

Informed Consent

All authors and relevant parties have reviewed and agreed to the contents of this manuscript.

The Corresponding Author is the primary point of contact for editorial communication and is responsible for coordinating submissions, revisions, and final approval of proofs.

Declaration of Interests

The authors confirm that there are no conflicts of interest associated with the submission of this manuscript. This assertion extends to all aspects of research, authorship, and publication processes. It has been determined that there are no financial or other relationships that could be interpreted as a potential conflict of interest influencing the outcomes of this work.